Impaired mineral ion metabolism in a mouse model of targeted calcium-sensing receptor (CaSR) deletion from vascular smooth muscle cells.

https://doi.org/10.1681/ASN.2021040585

https://jasn.asnjournals.org/content/early/2022/05/17/ASN.2021040585

Impaired mineral ion metabolism in a mouse model of targeted calcium-sensing receptor (CaSR) deletion from vascular smooth muscle cells

Martin Schepelmann[1,2], Marianna Ranieri[3], Irene Lopez-Fernandez[1], Thomas S. Webberley[1], Sarah C. Brennan[1,4], Polina L. Yarova,[1,5], Joao Graca[1,6], Umar-Khetaab Hanif[1], Christian Müller[2], Teresa Manhardt[2], Martina Salzmann[2], Helen Quasnichka[1], Sally A. Price[6], Donald T. Ward[7], Thierry Gilbert[8], Vladimir V. Matchkov[9], Robert A. Fenton[9], Amanda Herberger[10], Jenna Hwong[10], Christian Santa Maria[10], Chia-Ling Tu[10], Enikö Kallay[2], Giovanna Valenti[3], Wenhan Chang[10] and Daniela Riccardi[1].

1 School of Biosciences, Cardiff University, United Kingdom

2 Institute of Pathophysiology and Allergy Research, Medical University of Vienna, Austria

3 Department of Biosciences, Biotechnologies and Biopharmaceutics, University of Bari, Italy

4 Charles Perkins Centre, University of Sydney, NSW 2006, Australia

5 Translational & Clinical Research Institute, Newcastle University Medical School, Newcastle upon Tyne, UK

6 AstraZeneca, Macclesfield, Cheshire, United Kingdom

7 Division of Diabetes, Endocrinology & Gastroenterology, University of Manchester, Manchester, UK

8 Centre for Developmental Biology, University Paul Sabatier, Toulouse, FR

9 Department of Biomedicine, Aarhus University, Aarhus 8000, DK

10 Department of Medicine, University of California, San Francisco, CA, USA

Running title: Mineral ion dyshomeostasis in VSMC-CaSR knockout mice

Address correspondence to:

Wenhan Chang, PhD
University of California San Francisco
1700 Owens Street
San Francisco CA 94158, USA
Phone: (+1) 415-575-0558
Wenhan.Chang@ucsf.edu

Daniela Riccardi, PhD
School of Biosciences
The Sir Martin Evans Building, Cardiff University
Cardiff CF10 3AX, United Kingdom
Phone: (44) (0) 29 208 79132
riccardi@cardiff.ac.uk

Martin Schepelmann, PhD
Institute of Pathophysiology and Allergy Research
Medical University of Vienna
Währinger Gürtel 18-20, Leitstelle 3Q
1090, Vienna, Austria
Phone: (+43) 1 40400 51230
martin.schepelmann@meduniwien.ac.at

Significance statement

Chronic kidney disease (CKD) is associated with increased risk of mortality. In CKD, calcium and phosphate dyshomeostasis are associated with altered expression of the calcium-sensing receptor (CaSR) in the parathyroid glands and the kidney. The CaSR is also present in the vasculature, but its contribution to total body mineral ion homeostasis is unknown. Here we show that selective CaSR ablation from vascular smooth muscle cells (VSMC) leads to profound mineral ion imbalance in mice. These results demonstrate a hitherto undiscovered mode of mineral ion regulation outside the parathyroid glands and the kidneys. Alterations in VSMC-CaSR expression and activity would be expected to contribute to mineral ion imbalance in CKD.

Abstract

Background: Impaired mineral ion metabolism is a hallmark of chronic kidney disease (CKD) -metabolic bone disorder. It can lead to pathological vascular calcification (VC) and is associated with an increased risk of cardiovascular mortality. Loss of calcium sensing receptor (CaSR) expression in vascular smooth muscle cells (VSMCs) exacerbates VC *in vitro*; conversely, VC can be reduced by CaSR allosteric activators, calcimimetics.

Methods: To determine the role of the CaSR in VC, we characterized mice with targeted *Casr* gene knockout (KO) in VSMC ($^{SM22\alpha}$CaSR$^{\Delta flox/\Delta flox}$).

Results: VSMC cultured from KO mice calcified more readily than those from control (WT) mice i*n vitro.* However, KO mice did not show ectopic calcifications *in vivo* but a profound mineral ion imbalance. Specifically, KO mice exhibited hypercalcemia, hypercalciuria, hyperphosphaturia, and osteopenia, with elevated circulating FGF23, calcitriol (1,25-D_3), and PTH levels. Renal tubular, but not vascular α-Klotho protein expression was increased in KO mice. The observed phenotype of the KO mice could not be accounted for by altered CaSR expression in the kidney or the parathyroid glands.

Conclusions: These results suggest that the VSMC-CaSR directly contributes to total body mineral ion homeostasis, in addition to the established role of the receptor in the parathyroid-kidney-bone axis.

Introduction

Vascular calcification (VC) is a major complication in chronic kidney disease-metabolic bone disorder (CKD-MBD) and is an independent predictor of cardiovascular morbidity and mortality[1]. During VC, pro-contractile vascular smooth muscle cells (VSMC) undergo osteogenic transdifferentiation[2]. This process is exacerbated by altered mineral ion homeostasis in CKD-MBD patients[3, 4]. The CaSR is the key regulator of serum ionized calcium levels, *via* modulation of parathyroid hormone (PTH) secretion by the parathyroid glands (PTG) as well as Ca^{2+} reabsorption in the kidney[5]. Allosteric CaSR activators, calcimimetics, reduce plasma PTH and Ca^{2+} levels, decrease the prevalence of VC in animal studies of CKD[6, 7] and reduce cardiovascular events in older patients with moderate to severe hyperparathyroidism receiving hemodialysis[8]. However, the CaSR is also expressed in blood vessels where it may have a direct protective role against VC. We and others have shown that in VSMC, the CaSR is vasculoprotective, and that there is an inverse relationship between CaSR expression and VC[9, 10]. In uremic rats, administration of calcimimetics protects against VC[9-14]. CaSR expression is lost in cultured VSMC kept under pro-calcifying conditions *in vitro* and in calcified human arteries[9, 15] an effect which is, at least in part, restored by calcimimetic treatment[10, 12]. Over-expression of a "dominant negative" CaSR mutation accelerates calcification of isolated VSMC, which is prevented by calcimimetics[9]. However, there is a discrepancy between the preclinical *in vitro* observations and clinical findings about the role of the CaSR in VC. For instance, CaSR polymorphisms are not determinant of VC or cardiovascular outcomes in renal transplant patients[16], suggesting that the protective cardiovascular effects of calcimimetics in advanced CKD-MBD patients may also be modulated by additional systemic or local factor like PTH, vitamin D, and FGF23. Thus, the precise contribution of the vascular CaSR to pathological VC *in vivo* remains to be fully elucidated. To address this question directly, we studied mice with targeted *Casr* gene ablation in VSMC, in which we have previously

demonstrated a significant role of the receptor in the regulation of blood pressure and vascular tone[17].

Materials and Methods

Experimental animals

All animal procedures were approved by local ethical review and conformed with the regulations of the UK Home Office and/or the Animal Care and Use Committees of all the participating institutions. VSMC-specific CaSR knock-out mice were produced by breeding $CaSR^{flox/flox}$ mice, which carry 2 loxP sequences flanking exon 7 of the *Casr* gene[18], with SM22α (transgelin)-Cre mice. SM22α is transiently expressed during embryonic development in cardiac myocytes and, by mid-gestation, is confined to visceral and vascular SMCs[19]. Genotyping, husbandry, *etc*. are described in[17, 20]. $^{SM22a}CaSR^{\Delta flox/\Delta flox}$ mice (VSMC-CaSR knock-out, **KO**) and Cre-negative, $CaSR^{flox/flox}$ littermates (called "wild-type", for the wild-type CaSR; **WT**) were used for all experiments. Male mice only were used for all experiments, except for osmolality, soluble CaSR and bone metabolism marker measurements. All mice were on the same C57Bl/6 genetic background.

Culture media

Dulbecco's modified Eagle medium (DMEM) without $CaCl_2$, containing 1 mM phosphate, (Life Technologies, Grand Island, NY, USA) was supplemented with 1.2 mM $CaCl_2$, 50 U/ml penicillin-streptomycin, 2 mM L-glutamine, 10 % (v/v) fetal bovine serum (FBS), 1 mM Na-pyruvate and 1 % (v/v) amphotericin B solution (all Life Technologies) was used for the initial isolation of VSMCs (growth medium). For further culturing, the same medium was used but with omission of amphotericin B (culture medium). When indicated, the medium was supplemented with different concentrations of Ca^{2+} and inorganic phosphate (Pi) *via* addition of sterile 1M $CaCl_2$ solution and inorganic 1M phosphate buffer (NaH_2PO_4 / Na_2HPO_4) pH 7.4.

Primary VSMC isolation

VSMC were prepared according to published procedure[21] with modifications. In brief, mice were killed by cervical dislocation and the thoracic aorta was dissected. Aortas of 2-5 mice of the same genotype were pooled for one cell isolation and placed in growth medium and cleaned from the tunica adventitia and connective tissue. Segments of aorta ca. 1 mm in length were transferred to a culture flask and, after 10 minutes of drying / attaching in a tissue culture incubator, covered with growth medium and incubated at 37 °C / 95 % relative humidity / 5 % CO_2 until cells had grown out of the explants (ca. 2-4 weeks). The explants were then removed by aspiration and the cells were passaged using 0.05 % (v/v) trypsin-ethylenediaminetetraacetic (EDTA) solution in sterile phosphate-buffered saline, pH 7.4 (PBS) without $CaCl_2$ and $MgCl_2$ (all Life Technologies). Beginning with this passage VSMC culture medium was used instead of growth medium. Medium was changed every 3-4 days. Cells were used for experiments at passages 2-6. See **Figure S1** for a photograph array of the procedure.

Immunohistochemistry

Mouse organs were fixed by immersion in 4 % (w/v) paraformaldehyde (PFA) in PBS for 4 hours and 4 µm paraffin sections were cut and rehydrated according to standard protocols. Immunostainings were carried out to detect CaSR (1:500, MA1-934, Thermo Scientific, Loughborough, UK), TRPV5 (1:400, Alomone Labs, Jerusalem, Israel), Calbindin D-28k (1:3000, Sigma-Aldrich, Gillingham, UK), and PMCA 1/4 (1:100, Santa Cruz Biotechnology, Santa Cruz, USA). These immunostainings were carried out using a Ventana XT autostainer and OmnimapTM DAB reagents (Ventana, Tucson, USA). Hematoxylin (Clin-Tech, Guildford, UK) was used to counterstain the tissue sections, which were then dehydrated in ethanol, cleared in xylene, and mounted using Hystomount (TAAB Labs, Aldermaston, UK) or Fluoromount G (Thermo Fisher). Cyp27b1 and α-Klotho protein in aortas was detected using rabbit anti-Cyp27b1 (1:500, LSBio, Seattle, USA) and rabbit anti-klotho (1:200, Abcam)

antibodies, respectively. Antigen retrieval was performed by incubation for 20 min in 10 mM citrate buffer pH 6 in a steamer. Bound antibodies were visualized using the Dako Envision+ HRP rabbit kit (Agilent, Santa Clara, USA), nuclei were counterstained using Haematoxylin and mounted in Fluoromunt G. Tissue slides were scanned using a Scanscope® scanner (Aperio Technologies Incorporated, Vista, USA) or TissueFAXS Hard- and Software (TissueGnostics GmbH, Vienna, Austria). Quantitative evaluation of immunohistochemichal stainings was performed using ImageJ[22, 23], where % positive cells / positive area was counted after manual thresholding. For the aorta sections, mean color value for endothelium and smooth muscle layer were measured by subtracting the values of the negative controls for each aorta (IgG control) from the positively stained sections.

Immunofluorescence

Dissected organs were fixed by immersion in 4 % (w/v) PFA in PBS for 4 hours and then washed in PBS and stored in 30 % (w/v) sucrose in PBS at 4 °C for cryosections or dehydrated and paraffin embedded for paraffin sections. For cryosections, tissues were embedded in optimal cutting temperature compound (TissueTek OCT, Sakura-Finetek, Alphen aan den Rijn, NL) on dry ice and 8-10 µm sections were prepared using a cryo-microtome (Leica 2300L, Leica microsystems, Milton Keynes, UK). Rehydrated sections were incubated for 10 minutes in 50 mM NH_4Cl in PBS and then were antigen retrieved in 10 mM citrate buffer pH 6 for 15 minutes in a steamer followed by 5 minutes in 1 % sodium dodecyl sulphate (SDS) in PBS. Non-specific antibody binding was prevented by incubation in 1 % (w/v) BSA + 0.1 % (v/v) Tween 20 in PBS (blocking buffer) for 1 hour at room temperature. The CaSR was labelled by incubating the sections overnight with a rabbit-derived polyclonal antibody (1:100; AnaSpec, 53286, Fremont, CA, USA) or a mouse derived monoclonal antibody (1:500, clone 5C10, Abcam) in blocking buffer. Negative controls were performed by omission of the primary antibodies or replacement with an isotype control of rabbit IgG (Abcam). After washing in PBS,

primary antibody binding was visualized using appropriate Alexa Fluor fluorescence-dye coupled secondary anti IgG antibodies in a dilution of 1:500 in blocking buffer. High background was quenched by incubation of the sections in 0.2 mM Sudan Black B in 70 % ethanol for 10 minutes after the secondary antibody[24]. Nuclei were counterstained with Hoechst 34580 and slides were mounted using ProLong Gold® (all Life Technologies).

In vitro calcification assays

Cells were seeded in 24-well plates and were grown to 100 % confluency. The medium was then changed to growth medium supplemented with various $CaCl_2$ concentrations as specified in the results section. For induction of calcification, Pi (in the form of 1 M Na-phosphate buffer pH 7.4) were added to the culture medium. Cells were left in culture for 10 days and then fixed for 15 minutes in 4 % (w/v) PFA at room temperature. The amount of calcification was visualized by staining with 2 % alizarin red S (w/v) in water, pH 4.3, as described[25]. For quantification, after the incubation period, the cells were washed twice in PBS for and deposited calcium was extracted by decalcifying overnight in 0.6 N HCl at 37 °C. Eluted Ca^{2+} concentration was measured using the o-cresolphthalein complexone method[26, 27] and normalized against total protein concentration of the lysed cells (Pierce BCA assay; Thermo Fisher Scientific).

Ex vivo calcification of aortic explants

The assay was performed as described elsewhere[28]. In brief, aortas were dissected as described for the primary VSMC isolation. After cleaning the aortas from tunica adventitia, the endothelial layer was destroyed by stretching the tissue over the whole length. The vessel was then cut into 3-4 pieces of approximately equal length (5–8 mm). The pieces were incubated for 5 days in growth medium supplemented with varying of $CaCl_2$ concentrations (1.2–2.5 mM) and 3 mM inorganic phosphate, similarly to the VSMC calcification assays. Ca^{2+} concentrations were measured by o-cresolphthalein complexone method as described above and normalized

against the weight of the explants. Typical explant weights varied between 1.0 and 5.0 mg. Cryosections of 4 % (w/v) PFA fixed WT and KO aortas were stained for calcifications using Alizarin Red S as described above.

Parathyroid isolation and *ex vivo* PTH secretion

The *ex vivo* PTH-secretion assay in cultured mouse PTGs was adapted from[29]. Briefly, two mouse PTGs cleaned from surrounding tissues were submerged in a micro-droplet (10 µl) of secretion medium [SM, MEM Eagles with Earle's balanced salts supplemented with 0.5 mM Mg, 0.2 % bovine serum albumin, and 20 mM HEPES (pH 7.4)] and placed in the center of a 13 mm track-etched (0.1 µM pore) polycarbonate (PC) membrane, floating on a large drop (0.5 ml) of ice-cold SM supplemented with 3.0 mM Ca^{2+}. When all glands for the same experiment were dissected out, the PC membranes carrying the glands were transferred onto fresh drops of 37 °C SM containing 0.5 mM Ca^{2+} and equilibrated for ~45 minutes. Afterwards, the membrane with each pair of glands was transferred sequentially to a fresh drop (500 µl) of SM at 37 °C, increasing the Ca^{2+} concentration in the medium from 0.5 to 3.0 mM with 60 min for each concentration and a fresh medium change midway (at 30 minutes). Intact PTH released into the culture media was determined by ELISA (Quidel, San Diego, USA) in duplicate and used to calculate the rate of PTH release. For Ca^{2+} set-points, rates of PTH release were normalized to the rate at 0.5 mM Ca^{2+} and plotted against the Ca^{2+} concentration, and the PTH set-points (= EC_{50}) were deduced from the curve as the Ca^{2+} concentration which inhibits 50 % of the Ca^{2+}-suppressible PTH release.

Microcomputed tomography (µCT)

µCT was performed on distal femur for trabecular (Tb) bone and tibio-fibular junction (TFJ) for cortical (Ct) bone as described[29]. Briefly, femurs and tibiae fixed in 10 % phosphate-buffered formaldehyde (PBF) were scanned by a SCANCO vivaCT 100 scanner (SCANCO Medical AG, Basserdorf, Switzerland) with 10.5 µm voxel size and 55 kV X-ray energy. For

Tb bone in the distal femoral metaphysis, 100 serial cross-sectional scans (1.05 mm) of the secondary spongiosa were obtained from the end of the growth plate extending proximally. For Ct bone, 100 serial cross-sections (1.05 mm) of the tibia were obtained from the TFJ extending proximally. A threshold of 420 mg hydroxyapatite (HA)/mm^3 was applied to segment total mineralized bone matrix from soft tissue. Linear attenuation was calibrated using a µCT HA phantom. µCT image analysis and 3D reconstructions were done using the manufacturer's software to obtain the following structural parameters: Tb tissue volume (Tb.TV), Tb bone volume (Tb.BV), Tb.BV/TV ratio, Tb number (Tb.N), Tb connectivity density (Tb.CD), Tb thickness (Tb.Th), Tb spacing (Tb.Sp), Ct tissue volume (Ct.TV), and Ct thickness (Ct.Th).

Nephron count

One kidney per adult animal (16 weeks) was removed, decapsulated and immersed in 6M HCl at 37°C for 35 minutes. After several washes with tap water, the macerated kidney was stored at 4°C overnight. The tissue was homogenized with a glass-stirring rod and transferred to a 50 ml volumetric flask. Tap water was added to adjust the volume and the tubules and glomeruli suspension was then ready for nephron counting. One 0.5 ml aliquot was taken and deposited onto a glass slide with a millimeter mesh lattice to count the number of glomeruli. The total number of nephrons per kidney was calculated using the mean of 3 to 4 counts.

Tissue preparation for Western blot and RT-qPCR experiments

Mouse kidney slices were prepared as previously described[30]. In brief, WT and KO mice were euthanized by cervical dislocation. Kidneys were quickly removed and about 500 µm sections were made. Sectioned kidneys were equilibrated for 10 min in a specific kidney-slice buffer that contained 118 mM NaCl, 16 mM HEPES, 17 mM Na-HEPES, 14 mM glucose, 3.2 mM KCl, 2.5 mM $CaCl_2$, 1.8 mM $MgSO_4$, and 1.8 mM KH_2PO4 (pH 7.4) at 37°C. For Western blotting experiments, sections were then homogenized with a mini-potter in ice-cold kidney-slice buffer and Halt™ protease and phosphatase inhibitor Cocktail (Thermo Fisher, Rockford,

USA). Suspensions were centrifuged at 12,000 x *g* for 10 min at 4°C, and supernatants were loaded on acrylamide gels. Bones were prepared from hind-leg bones (femur, tibia and fibia) after cleaning of the surrounding connective tissue. After cleaning of the aortas from the tunica adventitia, the vessel was cut into 3-4 pieces, which were then processed accordingly.

For RT-PCR experiments, total RNA was extracted from kidneys, aorta and bones using Trizol reagent according to the manufacturer's instructions (Invitrogen, Life Technologies, Monza, Italy).

Gel Electrophoresis and Immunoblotting

Proteins were separated on 8-13 % bis-tris acrylamide gels under reducing conditions. Protein bands were electrophoretically transferred onto Immobilon-P membranes (Millipore Corporate Headquarters, Billerica, USA) for Western blot analysis, blocked in TBS-Tween-20 containing 3 % bovine serum albumin (BSA) and incubated with primary antibodies overnight.

Antibodies: polyclonal rabbit anti-CaSR (AnaSpec, this antibody had previously been determined to be most suitable for mouse tissue[31]), polyclonal rabbit anti-AQP2 (raised against 20-amino acids at the N-terminal, custom made from the polyphosphorylated region of rat AQP2)[32], polyclonal rabbit anti-AQP2-pS256 (a gift from Peter Deen)[33], polyclonal rabbit anti-AQP2-pS261 (Novus Biologicals, Littleton, Colorado, USA), polyclonal antibody against NaPi2a (Alpha Diagnostic Intl. Inc, San Antonio, Texas, USA), polyclonal rabbit anti-Klotho (Abcam, Cambridge, UK), monoclonal mouse anti-NCC (StressMarq Biosciences Inc., Victoria, CDN), polyclonal rabbit anti-β-actin (Cell Signaling Technology, Leiden, NL) and rabbit antibodies raised against the last 10 C-terminal amino acids (C-GANANRKFLD) of the E subunit of the V-ATPase (a gift from Dr Dennis Brown, Harvard Medical School, Boston, MA, USA). Secondary goat anti-rabbit or goat anti-mouse horseradish peroxidase–coupled antibodies were obtained from Santa Cruz Biotechnologies (Tebu-Bio, Milan, IT). Membranes were developed using Super Signal West Pico Chemiluminescent Substrate (Pierce, Rockford,

USA) with Chemidoc System (Bio-Rad Laboratories, Milan, Italy). Densitometry analysis was performed using Image Lab from Bio-Rad Laboratories, Inc. (Hercules, California, USA).

Real-Time PCR

Real-Time PCR experiments were performed to measure the relative expression of mRNA from WT and KO mouse kidneys, aorta, and bone. Total RNA was extracted using Trizol (Invitrogen, Life Technologies, Monza, Italy). Reverse transcription was performed on 1 µg of total RNA using SuperScript VILO Master Mix (Invitrogen, Life Technologies, Monza, Italy). Real-time PCR amplification was performed using TaqMan® Fast Advanced Master Mix with Aqp2 (ID number: Mm00437575_m1), CaSR (ID number: Mm00443375_m1), α-Klotho (ID number: Mm00502002_m1), NaPi2a (ID number: Mm00441450_m1), Tagln or Sm22α (ID number: Mm00441661_g1), FGF23 (ID number: Mm00445621_m1) and CYP27B1 or 1α-hydroxylase (ID number: Mm01165918_g1) assay, using GAPDH (ID number: Mm99999915_g1) and 18S (ID number: Hs99999901_s1) assay as housekeeping genes (Applied Biosystem, Life Technologies, Monza, Italy) in a StepOne Real-Time PCR System (Applied Biosystem, Life Technologies, Monza, Italy). Results were calculated according to the ΔΔCt method as relative expression to the average gene expression in the WT samples and then calculated as fold changes via $2^{-\Delta\Delta Ct}$.

Blood and urine collection, metabolic cages

Post-mortem blood collection from animals after neck dislocation was performed *via* cardiac puncture or retro-orbitally. Blood collection from live animals was performed *via* tail nick, as described [34]. K-EDTA, Na-heparin plasma and serum were collected in respective tubes (BD Biosciences, Oxford, UK). The blood was then centrifuged at 2,000 x *g* for 10 minutes and the supernatant stored at -80 °C. For urine collection, mice were weighed and transferred to metabolic cages (Tecniplast, Buguggiate, IT) and then left for 48 hours to allow them to acclimatize to the new environment. Mouse weight, food and water intake, as well as feces and

urine production were recorded over a period of 4 days. Samples from day 3 and 4 were then used for urine analysis and the results for both days were averaged. Urine was stored at -80 °C for further analysis.

Blood and urine analysis

Commercially available assays were used to measure plasma concentrations of Fetuin A (R&D Systems, Abingdon, UK), pyrophosphate (Abcam), FGF 23 (Kainos Laboratories, Tokyo, Japan), 1–84 PTH (Immutopics, San Clemente, USA), calcitriol (1,25-D_3) (Immunodiagnostic Systems, Tyne & Wear, UK), P1NP (Immunodiagnostic Systems), and TRAcP5b (Immunodiagnostic Systems), as well as serum concentration of soluble CaSR / N-terminal CaSR fragment (Elabscience, Wuhan, CN), and α-Klotho (cloud Clone Corp., Wuhan, CN). Concentrations of electrolytes were analyzed using a Roche modular P analyzer (Roche diagnostics) or, as were urea, creatinine, uric acid, glucose, and protein, by a commercially available clinical pathology service (MRC Harwell, Oxford, UK). Serum osmolality was measured using an Osmomat 30 (Gonotec, Berlin, DE) freezing point depression osmometer. Electrolyte concentrations for urine are reported as ion:creatinine ratio (abbreviated as ion:Cr), other clinical urine biomarkers (creatinine, total protein, urea and uric acid) are reported as excreted amount per day and total body weight (TBW). Urine osmolality was measured using a VAPRO® vapor pressure osmometer 5520 Wescor Inc., (Puteaux, France). Urine pH was measured using litmus paper with a range of pH between 2.0 and 9.0 (Macherey-Nagel, Düren, Germany). For urine precipitated analysis, 20 µl of urine were placed on the glass slide and covered with a coverslip. Samples were studies with phase contrast microscopy and analyzed qualitatively. Urinary AQP2 excretion was measured by ELISA as previously described[35, 36].

Statistical Analysis

All statistical analyses were performed using GraphPad Prism 8 (GraphPad Software, La Jolla, CA, USA). Statistical sample size is reported as N (number of separate experiments / biological

repeats) over n (technical repeats per sample, where applicable). Data are generally presented as mean ± SD, except for RT-qPCR data, which are shown as median ± interquartile range.

A difference of $p<0.05$ was considered statistically significant. The employed statistical tests and significance levels are specified in the respective results sections or in the figure legends.

Results

CaSR ablation induces calcification of VSMC *in vitro* but not *ex vivo* or *in vivo.*

Effectiveness of CaSR ablation from VSMC of $^{SM22\alpha}CaSR^{\Delta flox/\Delta flox}$ mice, at the molecular and functional levels, had already been confirmed previously[17, 37]. To test directly whether CaSR ablation prompts VSMCs to calcify, VSMC isolated from WT and KO mice were cultured in rising concentrations of Ca^{2+} (0.8–2.2 mM) and inorganic phosphate (Pi, 2–3 mM), spanning the (patho)physiological range. WT VSMC showed no calcification at 2 mM Pi at any Ca^{2+} concentration, while at 3 mM Pi, calcification was seen at ≥1.6 mM Ca^{2+}. In VSMC derived from KO aortae, calcification was significantly greater, and was already observed in 2 mM Pi at 1.6 mM Ca^{2+} or in 3 mM Pi at 1.2 mM Ca^{2+} (**Figure 1A**). Ca^{2+} incorporation in VSMC was Ca^{2+}-concentration dependent and was markedly more pronounced in VSMC from KO than in those from WT mice (**Figure 1B**). Furthermore, VSMC from WT and KO mice were cultured in 3 mM Pi and only 1.2 mM Ca^{2+}, so as to not saturate CaSR-activation, but in combination with 10 nM of the calcimimetic R-568. R-568 reduced calcium incorporation only in WT but not KO VSMC when compared to vehicle control (**Figure 1C**). Together, these results confirmed that the CaSR protects *in vitro* VSMC calcification.

Based on these observations, we had expected the KO mice to develop calcification in their blood vessels. However, there was no evidence of increased *in vivo* Ca^{2+} incorporation in the aortas of three-month-old KO mice compared to age matched WT controls. *Ex vivo* whole aortic explants from both six-month-old KO and WT mice, kept for ten days in 3 mM Pi and 1.8 mM

Ca^{2+} did not show any traceable calcification by alizarine red staining (**Figure S2**) and/or µCT (data not shown). Finally, as shown previously, aortas from up to 12-month-old WT and KO mice were histologically comparable and devoid of calcium deposits[17].

$^{SM22\alpha}$CaSR$^{\Delta flox/\Delta flox}$ mice exhibit impaired mineral ion homeostasis and alterations in calciotropic and phosphotropic hormones.

Blood biochemistry

Measurement of blood parameters, as shown in **Table 1**, showed moderate hypercalcemia and elevated plasma FGF23, PTH and 1,25-D_3 levels in 3-month-old mice. FGF23 and Ca^{2+} levels were also measured and found to be elevated in 18-month-old mice (**Table S1**) indicting that the mineral ion imbalance persists throughout the lifespan of the KO mice, without any apparent detrimental impact on their health. Serum α-Klotho-levels were comparable between both genotypes, at 3- and 18-months of age, although older mice had higher mean α-Klotho-levels than the younger ones.

Plasma Pi concentrations were reduced in 3-month-old KO compared to WT animals while Na^+, K^+, Cl^- and Mg^{2+} levels, and the levels of the physiological inhibitors of calcification, inorganic pyrophosphate (PPi) and Fetuin A were comparable between genotypes. Serum albumin levels were slightly decreased (pointing also towards a higher proportion of free ionized Ca^{2+} levels) while alkaline phosphatase (ALP) levels were increased in KO animals. Kidney function and hydration appeared to be normal in KO mice as urea and blood urea nitrogen (BUN), as well as hematocrit, did not differ from those of WT animals, while serum creatinine was slightly reduced in KO animals (**Table 1**). Serum osmolality assessed in the 18-month-old animals was unchanged between the two genotypes (**Table S1**). We also detected no difference in the concentration of "soluble" CaSR or rather N-terminal CaSR fragment between the genotypes in sera of 18-month-old animals (**Table S1**) which was comparable to

the level seen in serum of a 14-month-old non-genetically modified control (Ctrl) mouse. "Soluble" CaSR was around the lowest detection limit in sera of 3-month-old animals (**Figure S8**). These results exclude an antagonistic or hormonal effect of the truncated CaSR (encoded by exons 2-6) as the cause for the observed phenotype.

Metabolism, urine and organ weight

Urinary Ca^{2+}:Cr and Pi:Cr levels of KO were strongly elevated compared to WT animals (7.2-fold and 2.9-fold respectively), while Na^{+}:Cr, K^{+}:Cr, Cl^{-}:Cr and Mg^{2+}:Cr, creatinine, total protein, urea, uric acid, and glucose excretion ratios were comparable between the genotypes (**Table 2**). No differences in food consumption or fecal output were observed between genotypes. Water consumption and urine excretion were non-significantly elevated in KO mice compared to WT (**Table 2, Figure S3**).

Mineral ion and hormonal imbalance seen in $^{SM22\alpha}CaSR^{\Delta flox/\Delta flox}$ mice is not a direct consequence of altered gene/protein expression in the vasculature (aorta).

The observed phenotype points to a profound mineral ion dyshomeostasis in KO mice. We therefore investigated the expression of α-Klotho and 1α-hydroxylase since they are powerful regulators of mineral ion metabolism. mRNA expression of *α-Klotho*, *Cyp27b1,* and the smooth muscle marker *sm22α* were unchanged between WT and KO animals. CYP27B1 and α-Klotho protein expression levels were comparable between genotypes in both the endothelium and smooth muscle layers of the aorta (**Figure 2**). The cause of the observed mineral ion and hormonal imbalance in KO mice must therefore lie elsewhere.

$^{SM22\alpha}CaSR^{\Delta flox/\Delta flox}$ mice exhibit altered expression of renal α-Klotho and of Ca^{2+} and Pi transport proteins.

Renal expression of α-Klotho protein was significantly increased while that of the proximal tubule Na^+-dependent Pi transporter NaPi2a was significantly decreased in the kidneys of KO mice. The number of vitamin D receptor positive cells over whole kidney sections as determined by semi-quantitative immunohistochemistry analysis was comparable between genotypes, as was the mRNA expression of *Cyp27b1* (**Figure 3 and Figure S4**). The elevated plasma levels of 1,25-D_3 seen in KO mice could not be explained by the unchanged CYP27B1 protein expression in the kidney, which was comparable between genotypes (**Figure S5**), indicating extrarenal sources of 1,25-D_3. In supporting the action of 1,25-D_3 to increase urinary Ca^{2+} reabsorption[38], the expression of the epithelial Ca^{2+} channel TRPV5, the cytosolic Ca^{2+} buffer calbindin D28K, and the basolateral plasma membrane Ca^{2+}-ATPase (PMCA) was significantly increased in kidneys from KO compared to WT mice, as indicated by the larger area where staining intensities were above the threshold level (**Figure 3**).

Next, we confirmed that CaSR ablation from VSMC did not yield altered CaSR expression or gross anatomical changes in the kidney which could account for the observed phenotype. Renal CaSR mRNA and protein expression and distribution pattern (**Figure 3**, **Figure S6)** were all comparable between genotypes. There were no histomorphological differences between the kidneys of WT and KO mice of comparable age (**Figure S6A, B**). Kidney weights were comparable between WT and KO animals, both at 6 and 18 months of age (**Table S2**), as were nephron numbers (WT 30.54±5.21 *vs* KO 31.63±4.80 nephrons/mg kidney, mean±SD, N=7). Other organ weights (liver, stomach, spleen) were similar between genotypes, except for the hearts of 18-month-old KO animals, which were slightly heavier than those of age-matched WT animals (**Table S2**).

Urinary crystals, dilution and aquaporin expression levels of $^{SM22\alpha}CaSR^{\Delta flox/\Delta flox}$ mice.

The observed hypercalciuria and hyperphosphaturia could promote renal stone formation. While overt nephrolithiasis or nephrocalcinosis were not detected by histopathology, we did observe micro crystals in the urine of KO, but not WT animals (**Figure 4A**). Urine of KO mice had significantly reduced osmolality and pH compared to WT controls (**Figure 4**). The expression of the apical thiazide-sensitive Na^+-Cl^- cotransporter (NCC) and of the V-type H^+ ATPase were significantly increased in KO mouse kidneys, potentially leading to increased NaCl reabsorption and urine acidification respectively. Accordingly, the expression of the aquaporin-2 water channel (total AQP2) was significantly reduced in the kidneys of KO mice at both the mRNA and protein levels (**Figure S4** and **Figure 4F**). Specifically, the expression of the proteasome-sensitive phosphorylated form of AQP2, pS261[39], was upregulated while the active, vasopressin-stimulated pS256-AQP2[35] was downregulated in KO mice (**Figure 4G, H**), indicating a decreased amount of functional AQP2 resulting in decreased renal concentrating ability. In addition, urinary excretion of AQP2 was increased in KO animals (**Figure 4I**), pointing towards a higher degree of AQP2 degradation. Overall, KO mice had reduced urine concentrating ability, possibly as compensation to prevent kidney stone formation.

Hyperparathyroidism of $^{SM22\alpha}CaSR^{\Delta flox/\Delta flox}$ mice is neither due to altered CaSR expression, nor function, in the PTG.

VSMC-CaSR KO mice exhibit hypercalcemia and mild hyperparathyroidism (to reiterate, plasma total Ca^{2+}: 2.28 mmol / l *vs.* 2.94 mmol / l and PTH 151.7 *vs.* 256.6 pg/ml, WT *vs.* KO, see **Table 1**).To investigate whether the observed phenotype was due to partial ablation of the parathyroid CaSR, possibly through *SM22a* promoter leakage, we characterized CaSR expression and PTG function in the KO animals. PTGs from WT and KO animals were comparable in size and morphology (**Figure 5A**), as was the glands' CaSR expression (**Figure**

5B and C). Similarly, isolated PTGs had overlapping PTH secretion curves in response to rising levels of extracellular Ca^{2+} for both genotypes with identical IC_{50} values of ~ 1.1 mM Ca^{2+}_o (**Figure 5D**). Thus, the profound changes in mineral ion homeostasis seen in KO animals cannot be accounted for by altered CaSR expression, or function, in the PTGs.

$^{SM22a}CaSR^{\Delta flox/\Delta flox}$ mice exhibit elevated bone FGF23 levels and osteopenia.

The increased circulating levels of the phosphaturic hormone FGF23 are, at least in part, of skeletal origin, as FGF23 mRNA expression levels were increased in bones of KO mice (**Figure S7**). In contrast, FGF23 mRNA was undetectable in blood vessels of both genotypes (no amplification).

Micro-computerized tomography (µCT) on hind-leg bones of 3-month-old WT and KO mice revealed that especially trabecular bone quality was significantly reduced in KO animals compared to WT **(Table 3, Figure S7)**. These findings are in line with a significant increase in plasma levels of the bone resorption marker tartrate-resistant acid phosphatase 5b (TRAcP5b) in KO compared to WT animals, while the bone formation marker procollagen type 1 (P1NP) was comparable in both genotypes (**Figure S7**).

Discussion

Our data suggest that the CaSR protects VSMC from calcification *in vitro,* though loss of the VSMC-CaSR is apparently unable to induce detectable VC *in vivo*. Our mouse model further demonstrated that the VSMC-CaSR contributes directly to the regulation of mineral ion homeostasis, possibly by direct control of FGF23 and 1,25-D3 production / secretion, or indirectly through influencing the calcium-sensing or hormonal resistance in calciotropic organs. Most likely, the phenotype of the $^{SM22a}CaSR^{\Delta flox/\Delta flox}$ mouse is the result of a combination of disturbances acting together (**Figure 6**).

Vascular and VSMC calcification

VC is an independent predictor of cardiovascular morbidity and mortality in CKD-MBD patients[40, 41]. Previous observations in cultured human and bovine VSMC[9] indicated a direct role for the CaSR in preventing VSMC calcification / VC, which is substantiated by our findings on the effect and ability of CaSR ablation and calcimimetics to enhance and prevent VSMC calcification *in vitro*, respectively. These observations suggest that calcimimetics used clinically to treat patients with end-stage renal disease may reduce VC by directly targeting the vascular CaSR in addition to its action of improving mineral ion metabolism. However, the absence of VC in the aortae of KO mice *in vivo,* despite the animals' hypercalcemia, suggests that loss of CaSR expression is not sufficient to drive pathological VC.

An increase in 1α-hydroxylase expression in the vasculature promotes VC[42] but 1α-hydroxylase expression in the aortas of $^{SM22a}CaSR^{\Delta flox/\Delta flox}$ mice is not affected. High serum Pi levels are associated with greater prevalence of VC in patients with moderate CKD[43] whereas the $^{SM22a}CaSR^{\Delta flox/\Delta flox}$ were hypophosphatemic. Together with unchanged fetuin A and pyrophosphate (PPi) levels, potentially in combination with factors such as reduced vascular resistance in these animals[17], this may explain the lack of *in vivo* VC of $^{SM22a}CaSR^{\Delta flox/\Delta flox}$ mice.

Mineral ion metabolism imbalance

In addition to the previously described phenotype of reduced vascular contractility[17] and the changes in VSMC calcification behavior discussed above, we found that the $^{SM22a}CaSR^{\Delta flox/\Delta flox}$ mice also showed dysregulated mineral ion imbalance, manifesting in hypercalcemia, hypophosphatemia, hypercalciuria, hyperphosphaturia, and elevated FGF23, PTH, and 1,25-D_3 levels, together with increased bone resorption that is probably due to the chronically elevated PTH levels.

The phenotype is a direct consequence of VSMC-specific CaSR deletion

CaSR expression and / or function in PTG and kidney was not affected in the $^{SM22a}CaSR^{\Delta flox/\Delta flox}$ mice. Indeed, the phenotype of these mice cannot be explained by off-target CaSR deletion induced by our knock-out strategy, as constitutive or calciotropic organ specific CaSR deletion have very different phenotypes (**Table 4**). The global CaSR knock-out mouse exhibits severe hyperparathyroidism, growth retardation, and rarely lives longer than a few weeks[44] while the $^{SM22a}CaSR^{\Delta flox/\Delta flox}$ mice grow normally and have a normal lifespan. Using our strategy (Δexon 7), targeted deletion of the CaSR from the PTG was shown to induce a severe phenotype of hypercalcemia and hyperparathyroidism (~20-fold higher compared to controls)[18], along with PTGs whose secretion are totally unresponsive to rising Ca^{2+} concentrations[45]. The PTGs of the $^{SM22a}CaSR^{\Delta flox/\Delta flox}$ mice however were as responsive to extracellular Ca^{2+} as those from WT mice. A similar strategy (Δexon 3) was used to specifically delete the CaSR from the kidney, and these mice exhibit normal serum biochemistries and hypocalciuria[46]. Off-target effects of the truncated amino terminus of the CaSR are also highly unlikely, given that circulating levels of the (truncated) receptor were extremely low which would not be expected to interfere with the millimolar extracellular Ca^{2+} concentration, and that the residual truncated protein is by itself inactive and does not hinder the function of the native CaSR[18]. Collectively, these considerations suggest that the observed phenotype can only be reasonably accounted for by CaSR ablation from VSMC.

Features of the phenotype likely to be secondary to disturbed hormone secretion

The hypercalcemia of the $^{SM22a}CaSR^{\Delta flox/\Delta flox}$ mouse is most likely downstream to the increase in PTH and particularly 1,25-D_3 levels whereas the observed hypercalciuria is likely secondary to the hypercalcemia. $^{SM22a}CaSR^{\Delta flox/\Delta flox}$ mice also showed hyperphosphaturia and hypophosphatemia, likely *via* FGF23 and PTH induced down-regulation of NaPi2a and thus decreased phosphate reabsorption from the urine. The mildly increased PTH levels are also

plausibly the cause for reduced bone mineral density together with an increase in the bone resorption in the $^{SM22a}CaSR^{\Delta flox/\Delta flox}$ mice.

The underlying regulatory schemes become more complex when looking at the hormones themselves. The increase in 1,25-D_3 production could be secondary to the increase in PTH, though the hyperparathyroidism seems quite mild for such an effect. Also, given that the higher serum Pi would be expected to limit CaSR activation[47] by extracellular Ca^{2+}, the hypercalcemia and hypophosphatemia seen in the $^{SM22a}CaSR^{\Delta flox/\Delta flox}$ mice would provide optimal conditions for enhanced CaSR activation in the parathyroid and thus reduced PTH secretion, instead of hyperparathyroidism. These observations along with the unaltered Ca^{2+}-set point of PTH secretion from KO PTGs suggest that loss of CaSR in VSMC influences other mechanisms to promote PTH release *in vivo*.

The increase in 1,25-D_3 and PTH could then contribute to the elevated circulating FGF23 levels which are, at least in part, of skeletal origin given that FGF23 mRNA was undetectable in the aorta but was increased in the bones of $^{SM22a}CaSR^{\Delta flox/\Delta flox}$ mice.

Features of the phenotype likely to be caused by end-organ resistance

1,25-D_3 is a potent inducer of FGF23[48] and, conversely, FGF23 reduces the production of 1,25-D_3 by downregulating 1α-hydroxylase[49, 50] and by upregulating 24-hydroxylase[49]. However, in the $^{SM22a}CaSR^{\Delta flox/\Delta flox}$ mice, PTH and 1,25-D_3 levels were increased in KO mice despite the elevated FGF23 levels, indicating resistance of PTH and 1,25-D_3 synthesis to control by FGF23 and pointing away from FGF23 as sole primary factor. It is possible though that the high 1,25-D_3 and FGF23 levels actually mitigate PTH secretion, contributing to the only relatively mild increase in serum PTH in these mice – although there seems to be a degree of resistance to 1,25-D_3 and serum Ca^{2+} there as well. Taken together, given its resistance to control by FGF23, 1,25-D_3 could be the integrating element leading to the combined and complex phenotype observed in these mice.

However, FGF23 resistance does not seem to be a *general* feature of the $^{SM22a}CaSR^{\Delta flox/\Delta flox}$ mice, as regulation of renal phosphate reabsorption is apparently not affected. A factor that might play a role here is α-Klotho, which is acting both locally as co-factor for FGF23 and systemically in hormonal fashion[51]. Indeed, the observed hypercalcemia, elevated 1,25-D_3 and FGF23 levels and osteopenia of the $^{SM22a}CaSR^{\Delta flox/\Delta flox}$ mice are, except for the elevated PTH levels, somewhat reminiscent of the phenotype of the global Klotho$^{-/-}$ mice (**Table 4**). This suggests a common role for the VSMC-CaSR and α-Klotho in Ca^{2+} and Pi homeostasis, as already suggested by the biochemical interaction between CaSR and α-Klotho in the PTG[52] and in the kidney[53]. The kidney is the major site of α-Klotho production[54] where changes in serum and urinary α-Klotho mirror those of renal α-Klotho levels[55]. Interestingly, in the $^{SM22a}CaSR^{\Delta flox/\Delta flox}$ mice, even though renal α-Klotho levels were increased, vascular or circulating α-Klotho levels were not affected, suggesting that absence of CaSR from VSMC influences circulating and local α-Klotho metabolism differently.

Elevated serum FGF23 may be an independent predictor of cardiovascular mortality[56]. Experimentally, FGF23 alone can directly induce LVH[57] and FGF23 gain of function leads to volume expansion, hypertension, and cardiac hypertrophy[58]. Despite chronically elevated FGF23 levels, our $^{SM22a}CaSR^{\Delta flox/\Delta flox}$ mice did not develop LVH at 14 months of age and we did not observe increased mortality[17, 37]. Since these mice are hypotensive despite their chronically elevated FGF23 levels, vascular contractility may play a larger role here than FGF23 mediated renal and cardiac effects on blood pressure.

Renal phenotype

The expression of TRPV5, calbindin D28K and PMCA were all increased in the kidneys of the $^{SM22a}CaSR^{\Delta flox/\Delta flox}$ mice, suggesting higher transcellular Ca^{2+} reabsorption. This increase, due to chronic elevation of 1,25-D_3, PTH, and FGF23[58] levels, may contribute to their hypercalcemia, whereas the increased renal NCC expression is likely to contribute to the

observed hypercalciuria, as serum and urine Mg^{2+} levels were unaffected in KO mice, suggesting that the abnormality indeed lies within the NCC-expressing distal convoluted tubule[59], rather than the thick ascending limb, where Ca^{2+} and Mg^{2+} reabsorption happen in parallel driven by the transepithelial potential difference[60].

The hypercalciuria and hyperphosphaturia of the $^{SM22a}CaSR^{\Delta flox/\Delta flox}$ mice could be the cause for the formation of the observed micro crystals in their urine. We did not observe nephrolithiasis in these animals, which can be explained by a CaSR-mediated compensatory mechanism of urine dilution and acidification. In the collecting duct principal cells, the CaSR[61] is co-expressed luminally with AQP2[39, 62-65], and decreases water reabsorption by reducing the apical insertion of AQP2 water channels. In intercalated cells, the CaSR induces luminal acidification by activating the V-type H^+ ATPase. In $^{SM22a}CaSR^{\Delta flox/\Delta flox}$ mice, renal AQP2 expression levels were reduced while urinary excretion of degraded AQP2 was increased, indicating decreased water reabsorption, and explaining the reduction of urine osmolality. Furthermore, renal V-ATPase expression was increased in $^{SM22a}CaSR^{\Delta flox/\Delta flox}$ mice compared to WT controls, explaining their acidified urine.

Implications and conclusions

Our study may also have important clinical implications. Physiological pulsation is necessary for the maintenance of CaSR expression in human aortic smooth muscle cells and may protect arteries from developing VC[66]. Thus, in early CKD, an increase in arterial stiffness and blood pressure, could potentially yield a reduction in CaSR expression by VSMC. While absence of the CaSR apparently does not prompt immediate VC in the blood vessels *in vivo*, it could contribute to the disease onset *via* the deleterious effects of VSMC-CaSR loss on mineral ion homeostasis, as observed in our mouse model. A reduction in blood pressure could thus slow the VSMC-CaSR loss-induced disease progression. Furthermore, a reduction in blood pressure below what is recommended by most guidelines led to improved cardiovascular and all-cause

mortality in the CKD population[67]. Our study supports these findings and points to an early targeting of blood pressure control to delay CKD progression. Owing to their ability to affect the VSMC-CaSR, calcimimetics would also be expected to be directly vasculoprotective, in addition to their systemic effects mediated by suppression of circulating PTH and FGF23 levels.

The VSMC-CaSR apparently contributes to mineral ion homeostasis control, possibly by direct control of FGF23 and 1,25-D_3 production / secretion, though the phenotype of the $^{SM22a}CaSR^{\Delta flox/\Delta flox}$ mouse is likely to be the result of a combination of disturbances acting together. Global deletion of the CaSR from VSMC might affect calcium-sensing in all calciotropic organs to some degree, suggesting a role for the VSMC-CaSR in contributing to each individual organ's response to mineral ion homeostasis. Further work will be necessary to dissect the organ-specific paracrine/autocrine responses *vs* whole body endocrine feedback mechanisms for the fine control of mineral ion homeostasis that the VSMC-CaSR evidently supports.

Author contributions

DR, WC, and MSch designed the study;
MSch, MR, ILF, TSW, SCB, PLY, JG, TM, MSa, CLT, CM, HQ, SAP, DTW, TG, VVM, RAF, AH, JH, CSM and WC carried out experiments;
MSch, MR, TSW, CM, RAF, UKH, DTW, VVM, TG, CSM, JH, WC, EK and GV analyzed the data;
MSch, MR, TSW and WC made the figures;
MSch, MR, WC, SCB, GV, SAP, VVM, RAF, EK and DR drafted and revised the paper;
All authors approved the final version of the manuscript.

Acknowledgements

The authors want to acknowledge B. Monk, B. van der Kolk, A. Wheatley, P. Edwards, and N. Kupper for their help with some of the initial experiments and revisions, and Professor AE Canfield and Dr B. Richards for helpful discussions.

Disclosures

The authors have no disclosures and no competing financial interests.

Funding

EU Marie Curie Innovative Training Network Grant FP7-264663 “Multifaceted CaSR” (to DR, SAP and EK), Austrian Science Fund P-29948-B28 (to EK), Austrian Science Fund and Herzfelder’sche Familienstiftung P-32840-B (to MSch), “Intervento cofinanziato dal Fondo di Sviluppo e Coesione 2007-2013–APQ Ricerca Regione Puglia, Programma Regionale a Sostegno della Specializzazione Intelligente e della Sostenibilità Sociale ed Ambientale – FutureInResearch.” CHVNKZ4 (to MR), Kidney Research UK (Intercalated Scholarship) (to UKH), NIH R01DK12165601, R01DK122259, and VA-BLR&D I01BX005851 and 1IK6BX004835 (to WC).

References

1. London GM, Marchais SJ, Guerin AP, Metivier F: Arteriosclerosis, vascular calcifications and cardiovascular disease in uremia. *Curr Opin Nephrol Hypertens,* 14**:** 525-531, 2005
2. Villa-Bellosta R, Millan A, Sorribas V: Role of calcium-phosphate deposition in vascular smooth muscle cell calcification. *Am J Physiol Cell Physiol,* 300**:** C210-220, 2011 10.1152/ajpcell.00229.2010
3. Yamada S, Giachelli CM: Vascular calcification in CKD-MBD: Roles for phosphate, FGF23, and Klotho. *Bone,* 100**:** 87-93, 2017 10.1016/j.bone.2016.11.012
4. Block GA, Klassen PS, Lazarus JM, Ofsthun N, Lowrie EG, Chertow GM: Mineral metabolism, mortality, and morbidity in maintenance hemodialysis. *J Am Soc Nephrol,* 15**:** 2208-2218, 2004 10.1097/01.ASN.0000133041.27682.A2
5. Riccardi D, Valenti G: Localization and function of the renal calcium-sensing receptor. *Nat Rev Nephrol,* 12**:** 414-425, 2016 10.1038/nrneph.2016.59
6. Yu L, Tomlinson JE, Alexander ST, Hensley K, Han CY, Dwyer D, et al.: Etelcalcetide, A Novel Calcimimetic, Prevents Vascular Calcification in A Rat Model of Renal Insufficiency with Secondary Hyperparathyroidism. *Calcif Tissue Int,* 101**:** 641-653, 2017 10.1007/s00223-017-0319-7
7. Moe SM, Seifert MF, Chen NX, Sinders RM, Chen X, Duan D, et al.: R-568 reduces ectopic calcification in a rat model of chronic kidney disease-mineral bone disorder (CKD-MBD). *Nephrol Dial Transplant,* 24**:** 2371-2377, 2009 10.1093/ndt/gfp078
8. Parfrey PS, Drueke TB, Block GA, Correa-Rotter R, Floege J, Herzog CA, et al.: The Effects of Cinacalcet in Older and Younger Patients on Hemodialysis: The Evaluation of Cinacalcet HCl Therapy to Lower Cardiovascular Events (EVOLVE) Trial. *Clin J Am Soc Nephrol,* 10**:** 791-799, 2015 10.2215/CJN.07730814
9. Alam MU, Kirton JP, Wilkinson FL, Towers E, Sinha S, Rouhi M, et al.: Calcification is associated with loss of functional calcium-sensing receptor in vascular smooth muscle cells. *Cardiovasc Res,* 81**:** 260-268, 2009 10.1093/cvr/cvn279
10. Henaut L, Boudot C, Massy ZA, Lopez-Fernandez I, Dupont S, Mary A, et al.: Calcimimetics increase CaSR expression and reduce mineralization in vascular smooth muscle cells: mechanisms of action. *Cardiovasc Res,* 101**:** 256-265, 2014 10.1093/cvr/cvt249
11. Ciceri P, Elli F, Brenna I, Volpi E, Brancaccio D, Cozzolino M: The Calcimimetic Calindol Prevents High Phosphate-Induced Vascular Calcification by Upregulating Matrix GLA Protein. *Nephron Exp Nephrol,* 122**:** 75-82, 2013 10.1159/000349935
12. Ciceri P, Volpi E, Brenna I, Elli F, Borghi E, Brancaccio D, et al.: The combination of lanthanum chloride and the calcimimetic calindol delays the progression of vascular smooth muscle cells calcification. *Biochem Biophys Res Commun,* 418**:** 770-773, 2012 10.1016/j.bbrc.2012.01.097
13. Koleganova N, Piecha G, Ritz E, Schmitt CP, Gross ML: A calcimimetic (R-568), but not calcitriol, prevents vascular remodeling in uremia. *Kidney Int,* 75**:** 60-71, 2009 10.1038/ki.2008.490
14. Mendoza FJ, Martinez-Moreno J, Almaden Y, Rodriguez-Ortiz ME, Lopez I, Estepa JC, et al.: Effect of calcium and the calcimimetic AMG 641 on matrix-Gla protein in vascular smooth muscle cells. *Calcif Tissue Int,* 88**:** 169-178, 2011 10.1007/s00223-010-9442-4
15. Molostvov G, James S, Fletcher S, Bennett J, Lehnert H, Bland R, et al.: Extracellular calcium-sensing receptor is functionally expressed in human artery. *Am J Physiol Renal Physiol,* 293**:** F946-955, 2007 10.1152/ajprenal.00474.2006
16. Babinsky VN, Hannan FM, Youhanna SC, Marechal C, Jadoul M, Devuyst O, et al.: Association studies of calcium-sensing receptor (CaSR) polymorphisms with serum

concentrations of glucose and phosphate, and vascular calcification in renal transplant recipients. *PloS one,* 10**:** e0119459, 2015 10.1371/journal.pone.0119459
17. Schepelmann M, Yarova PL, Lopez-Fernandez I, Davies TS, Brennan SC, Edwards PJ, et al.: The vascular Ca2+-sensing receptor regulates blood vessel tone and blood pressure. *Am J Physiol Cell Physiol,* 310**:** C193-204, 2016 10.1152/ajpcell.00248.2015
18. Chang W, Tu C, Chen TH, Bikle D, Shoback D: The extracellular calcium-sensing receptor (CaSR) is a critical modulator of skeletal development. *Sci Signal,* 1**:** ra1, 2008 10.1126/scisignal.1159945
19. Holtwick R, Gotthardt M, Skryabin B, Steinmetz M, Potthast R, Zetsche B, et al.: Smooth muscle-selective deletion of guanylyl cyclase-A prevents the acute but not chronic effects of ANP on blood pressure. *Proc Natl Acad Sci U S A,* 99**:** 7142-7147, 2002 10.1073/pnas.102650499
20. Yarova PL, Stewart AL, Sathish V, Britt RD, Jr., Thompson MA, AP PL, et al.: Calcium-sensing receptor antagonists abrogate airway hyperresponsiveness and inflammation in allergic asthma. *Science translational medicine,* 7**:** 284ra260, 2015 10.1126/scitranslmed.aaa0282
21. Sage AP, Lu J, Tintut Y, Demer LL: Hyperphosphatemia-induced nanocrystals upregulate the expression of bone morphogenetic protein-2 and osteopontin genes in mouse smooth muscle cells in vitro. *Kidney Int,* 79**:** 414-422, 2011 10.1038/ki.2010.390
22. Schneider CA, Rasband WS, Eliceiri KW: NIH Image to ImageJ: 25 years of image analysis. *Nat Methods,* 9**:** 671-675, 2012
23. Schindelin J, Arganda-Carreras I, Frise E, Kaynig V, Longair M, Pietzsch T, et al.: Fiji: an open-source platform for biological-image analysis. *Nat Methods,* 9**:** 676-682, 2012 10.1038/nmeth.2019
24. Sun Y, Yu H, Zheng D, Cao Q, Wang Y, Harris D, et al.: Sudan black B reduces autofluorescence in murine renal tissue. *Arch Pathol Lab Med,* 135**:** 1335-1342, 2011 10.5858/arpa.2010-0549-OA
25. Puchtler H, Meloan SN, Terry MS: On the history and mechanism of alizarin and alizarin red S stains for calcium. *J Histochem Cytochem,* 17**:** 110-124, 1969
26. Jono S, Nishizawa Y, Shioi A, Morii H: Parathyroid hormone-related peptide as a local regulator of vascular calcification. Its inhibitory action on in vitro calcification by bovine vascular smooth muscle cells. *Arterioscler Thromb Vasc Biol,* 17**:** 1135-1142, 1997
27. Moorehead WR, Biggs HG: 2-Amino-2-methyl-1-propanol as the alkalizing agent in an improved continuous-flow cresolphthalein complexone procedure for calcium in serum. *Clin Chem,* 20**:** 1458-1460, 1974
28. Leroux-Berger M, Queguiner I, Maciel TT, Ho A, Relaix F, Kempf H: Pathologic calcification of adult vascular smooth muscle cells differs on their crest or mesodermal embryonic origin. *J Bone Miner Res,* 26**:** 1543-1553, 2011 10.1002/jbmr.382
29. Cheng Z, Liang N, Chen TH, Li A, Santa Maria C, You M, et al.: Sex and age modify biochemical and skeletal manifestations of chronic hyperparathyroidism by altering target organ responses to Ca2+ and parathyroid hormone in mice. *J Bone Miner Res,* 28**:** 1087-1100, 2013 10.1002/jbmr.1846
30. Ranieri M, Tamma G, Di Mise A, Russo A, Centrone M, Svelto M, et al.: Negative feedback from CaSR signaling to aquaporin-2 sensitizes vasopressin to extracellular Ca2. *Journal of cell science,* 128**:** 2350-2360, 2015 10.1242/jcs.168096
31. Graca JA, Schepelmann M, Brennan SC, Reens J, Chang W, Yan P, et al.: Comparative expression of the extracellular calcium-sensing receptor in the mouse, rat, and human kidney. *Am J Physiol Renal Physiol,* 310**:** F518-533, 2016 10.1152/ajprenal.00208.2015
32. Tamma G, Lasorsa D, Ranieri M, Mastrofrancesco L, Valenti G, Svelto M: Integrin signaling modulates AQP2 trafficking via Arg-Gly-Asp (RGD) motif. *Cellular*

physiology and biochemistry : international journal of experimental cellular physiology, biochemistry, and pharmaco, 27**:** 739-748, 2011 10.1159/000330082
33. Trimpert C, van den Berg DT, Fenton RA, Klussmann E, Deen PM: Vasopressin increases S261 phosphorylation in AQP2-P262L, a mutant in recessive nephrogenic diabetes insipidus. *Nephrology, dialysis, transplantation : official publication of the European Dialysis and Transplant Associatio,* 27**:** 4389-4397, 2012 10.1093/ndt/gfs292
34. Sadler AM, Bailey SJ: Validation of a refined technique for taking repeated blood samples from juvenile and adult mice. *Lab Anim,* 47**:** 316-319, 2013 10.1177/0023677213494366
35. Procino G, Mastrofrancesco L, Tamma G, Lasorsa DR, Ranieri M, Stringini G, et al.: Calcium-sensing receptor and aquaporin 2 interplay in hypercalciuria-associated renal concentrating defect in humans. An in vivo and in vitro study. *PloS one,* 7**:** e33145, 2012 10.1371/journal.pone.0033145
36. Tamma G, Di Mise A, Ranieri M, Svelto M, Pisot R, Bilancio G, et al.: A decrease in aquaporin 2 excretion is associated with bed rest induced high calciuria. *J Transl Med,* 12**:** 133, 2014 10.1186/1479-5876-12-133
37. Yarova PL, Stewart AL, Sathish V, Britt RD, Jr., Thompson MA, AP PL, et al.: Calcium-sensing receptor antagonists abrogate airway hyperresponsiveness and inflammation in allergic asthma. *Sci Transl Med,* 7**:** 284ra260, 2015 10.1126/scitranslmed.aaa0282
38. Alexander RT, Woudenberg-Vrenken TE, Buurman J, Dijkman H, van der Eerden BC, van Leeuwen JP, et al.: Klotho prevents renal calcium loss. *J Am Soc Nephrol,* 20**:** 2371-2379, 2009 10.1681/ASN.2008121273
39. Ranieri M, Zahedi K, Tamma G, Centrone M, Di Mise A, Soleimani M, et al.: CaSR signaling down-regulates AQP2 expression via a novel microRNA pathway in pendrin and NaCl cotransporter knockout mice. *FASEB J,* 32**:** 2148-2159, 2018 10.1096/fj.201700412RR
40. London GM, Guerin AP, Marchais SJ, Metivier F, Pannier B, Adda H: Arterial media calcification in end-stage renal disease: impact on all-cause and cardiovascular mortality. *Nephrol Dial Transplant,* 18**:** 1731-1740, 2003 10.1093/ndt/gfg414
41. Raggi P, Boulay A, Chasan-Taber S, Amin N, Dillon M, Burke SK, et al.: Cardiac calcification in adult hemodialysis patients. A link between end-stage renal disease and cardiovascular disease? *J Am Coll Cardiol,* 39**:** 695-701, 2002 10.1016/s0735-1097(01)01781-8
42. Torremade N, Bozic M, Panizo S, Barrio-Vazquez S, Fernandez-Martin JL, Encinas M, et al.: Vascular Calcification Induced by Chronic Kidney Disease Is Mediated by an Increase of 1alpha-Hydroxylase Expression in Vascular Smooth Muscle Cells. *J Bone Miner Res,* 31**:** 1865-1876, 2016 10.1002/jbmr.2852
43. Adeney KL, Siscovick DS, Ix JH, Seliger SL, Shlipak MG, Jenny NS, et al.: Association of serum phosphate with vascular and valvular calcification in moderate CKD. *J Am Soc Nephrol,* 20**:** 381-387, 2009 10.1681/ASN.2008040349
44. Ho C, Conner DA, Pollak MR, Ladd DJ, Kifor O, Warren HB, et al.: A mouse model of human familial hypocalciuric hypercalcemia and neonatal severe hyperparathyroidism. *Nat Genet,* 11**:** 389-394, 1995 10.1038/ng1295-389
45. Chang W, Tu CL, Jean-Alphonse FG, Herberger A, Cheng Z, Hwong J, et al.: PTH hypersecretion triggered by a GABAB1 and Ca(2+)-sensing receptor heterocomplex in hyperparathyroidism. *Nat Metab,* 2**:** 243-255, 2020 10.1038/s42255-020-0175-z
46. Toka HR, Al-Romaih K, Koshy JM, DiBartolo S, 3rd, Kos CH, Quinn SJ, et al.: Deficiency of the calcium-sensing receptor in the kidney causes parathyroid hormone-independent hypocalciuria. *J Am Soc Nephrol,* 23**:** 1879-1890, 2012 10.1681/ASN.2012030323

47. Centeno PP, Herberger A, Mun HC, Tu C, Nemeth EF, Chang W, et al.: Phosphate acts directly on the calcium-sensing receptor to stimulate parathyroid hormone secretion. *Nat Commun,* 10**:** 4693, 2019 10.1038/s41467-019-12399-9
48. Saito H, Maeda A, Ohtomo S, Hirata M, Kusano K, Kato S, et al.: Circulating FGF-23 is regulated by 1alpha,25-dihydroxyvitamin D3 and phosphorus in vivo. *J Biol Chem,* 280**:** 2543-2549, 2005 10.1074/jbc.M408903200
49. Shimada T, Hasegawa H, Yamazaki Y, Muto T, Hino R, Takeuchi Y, et al.: FGF-23 is a potent regulator of vitamin D metabolism and phosphate homeostasis. *J Bone Miner Res,* 19**:** 429-435, 2004 10.1359/JBMR.0301264
50. Shimada T, Kakitani M, Yamazaki Y, Hasegawa H, Takeuchi Y, Fujita T, et al.: Targeted ablation of Fgf23 demonstrates an essential physiological role of FGF23 in phosphate and vitamin D metabolism. *J Clin Invest,* 113**:** 561-568, 2004 10.1172/JCI19081
51. Dalton GD, Xie J, An SW, Huang CL: New Insights into the Mechanism of Action of Soluble Klotho. *Front Endocrinol (Lausanne),* 8**:** 323, 2017 10.3389/fendo.2017.00323
52. Fan Y, Liu W, Bi R, Densmore MJ, Sato T, Mannstadt M, et al.: Interrelated role of Klotho and calcium-sensing receptor in parathyroid hormone synthesis and parathyroid hyperplasia. *Proc Natl Acad Sci U S A,* 115**:** E3749-E3758, 2018 10.1073/pnas.1717754115
53. Yoon J, Liu Z, Lee E, Liu L, Ferre S, Pastor J, et al.: Physiologic Regulation of Systemic Klotho Levels by Renal CaSR Signaling in Response to CaSR Ligands and pHo. *J Am Soc Nephrol,* 2021 10.1681/ASN.2021020276
54. Kuro-o M, Matsumura Y, Aizawa H, Kawaguchi H, Suga T, Utsugi T, et al.: Mutation of the mouse klotho gene leads to a syndrome resembling ageing. *Nature,* 390**:** 45-51, 1997 10.1038/36285
55. Hu MC, Shi M, Zhang J, Quinones H, Griffith C, Kuro-o M, et al.: Klotho deficiency causes vascular calcification in chronic kidney disease. *J Am Soc Nephrol,* 22**:** 124-136, 2011 10.1681/ASN.2009121311
56. Arnlov J, Carlsson AC, Sundstrom J, Ingelsson E, Larsson A, Lind L, et al.: Serum FGF23 and risk of cardiovascular events in relation to mineral metabolism and cardiovascular pathology. *Clin J Am Soc Nephrol,* 8**:** 781-786, 2013 10.2215/CJN.09570912
57. Faul C, Amaral AP, Oskouei B, Hu MC, Sloan A, Isakova T, et al.: FGF23 induces left ventricular hypertrophy. *J Clin Invest,* 121**:** 4393-4408, 2011 10.1172/JCI46122
58. Andrukhova O, Slavic S, Smorodchenko A, Zeitz U, Shalhoub V, Lanske B, et al.: FGF23 regulates renal sodium handling and blood pressure. *EMBO Mol Med,* 6**:** 744-759, 2014 10.1002/emmm.201303716
59. Subramanya AR, Ellison DH: Distal convoluted tubule. *Clin J Am Soc Nephrol,* 9**:** 2147-2163, 2014 10.2215/CJN.05920613
60. de Rouffignac C, Quamme G: Renal magnesium handling and its hormonal control. *Physiol Rev,* 74**:** 305-322, 1994 10.1152/physrev.1994.74.2.305
61. Renkema KY, Velic A, Dijkman HB, Verkaart S, van der Kemp AW, Nowik M, et al.: The calcium-sensing receptor promotes urinary acidification to prevent nephrolithiasis. *J Am Soc Nephrol,* 20**:** 1705-1713, 2009 10.1681/ASN.2008111195
62. Ranieri M: Renal Ca(2+) and Water Handling in Response to Calcium Sensing Receptor Signaling: Physiopathological Aspects and Role of CaSR-Regulated microRNAs. *Int J Mol Sci,* 20, 2019 10.3390/ijms20215341
63. Sands JM, Naruse M, Baum M, Jo I, Hebert SC, Brown EM, et al.: Apical extracellular calcium/polyvalent cation-sensing receptor regulates vasopressin-elicited water permeability in rat kidney inner medullary collecting duct. *J Clin Invest,* 99**:** 1399-1405, 1997 10.1172/JCI119299

64. Riccardi D, Brown EM: Physiology and pathophysiology of the calcium-sensing receptor in the kidney. *Am J Physiol Renal Physiol,* 298**:** F485-499, 2010 10.1152/ajprenal.00608.2009
65. Brown EM: Physiology and pathophysiology of the extracellular calcium-sensing receptor. *Am J Med,* 106**:** 238-253, 1999
66. Molostvov G, Hiemstra TF, Fletcher S, Bland R, Zehnder D: Arterial Expression of the Calcium-Sensing Receptor Is Maintained by Physiological Pulsation and Protects against Calcification. *PloS one,* 10**:** e0138833, 2015 10.1371/journal.pone.0138833
67. Gosmanova EO, Kovesdy CP: Blood Pressure Targets in CKD: Lessons Learned from SPRINT and Previous Observational Studies. *Curr Cardiol Rep,* 18**:** 88, 2016 10.1007/s11886-016-0769-y
68. Kaludjerovic J, Komaba H, Lanske B: Effects of klotho deletion from bone during chronic kidney disease. *Bone,* 100**:** 50-55, 2017 10.1016/j.bone.2017.02.006

Supplemental Material Table of Contents

Page numbers refer to the *supplemental material_revised.pdf*

Tables

Table 1: Blood biochemistry of 3-month-old WT and KO mice. 1,25-D_3 = 1,25-dihydroxy vitamin D / calcitriol, BUN = blood urea nitrogen. * $p < 0.05$, ** $p < 0.01$, *** $p < 0.001$, mean ± SD, two-tailed T-test.

Parameter	Unit	WT	N	KO	N	*p*-value	
Na^+	mmol / l	145.35 ± 2.77	17	144.15 ± 3.84	10	0.3540	
Cl^-	mmol / l	109.18 ± 3.34	17	108.45 ± 4.82	10	0.6472	
K^+	mmol / l	5.24 ± 0.40	3	5.62 ± 0.18	3	0.2092	
Ca^{2+}	mmol / l	2.28 ± 0.21	28	2.94 ± 0.59	21	<0.0001	***
Mg^{2+}	mmol / l	1.06 ± 0.12	22	1.15 ± 0.22	20	0.0979	
FGF23	pg / ml	145.0 ± 36.4	11	384.4 ± 204.5	6	0.0015	**
Pi	mmol / l	2.36 ± 0.45	17	1.94 ± 0.47	16	0.0146	*
Hematocrit	%	40.3 ± 7.6	9	38.9 ± 8.6	6	0.7407	
PTH	pg / ml	151.7 ± 115.5	30	256.6 ± 249.8	30	0.0411	*
1,25-D_3	pmol / l	162.1 ± 81.3	19	310.8 ± 173.4	17	0.0020	**
α-Klotho	pg / ml	555.4 ± 164.6	13	564.7 ± 389.3	11	0.9379	
Aldosterone	pg / ml	508.1 ± 199.0	12	421.8 ± 205.2	12	0.3072	
Renin	pg / ml	123.8 ± 58.0	12	115.4 ± 40.3	12	0.6850	
Fetuin A	µg / ml	201.4 ± 40.9	12	193.0 ± 40.8	12	0.6175	
PPi	µmol / l	34.1 ± 40.8	12	25.0 ± 14.2	12	0.4747	
Albumin	mg / ml	29.4 ± 1.4	11	27.6 ± 1.7	11	0.0179	*
ALP	U / l	81.73 ± 11.38	11	100.18 ± 22.74	11	0.0297	*
Creatinine	µmol / l	15.4 ± 1.6	6	13.0 ± 1.3	5	0.0265	*
Urea	mmol / l	10.1 ± 1.3	6	10.4 ± 0.3	5	0.6474	
BUN	mmol / l	8.4 ± 2.4	11	8.7 ± 1.8	11	0.7781	
Total Protein	mg / ml	54.4 ± 3.0	6	51.2 ± 2.6	4	0.1196	

Table 2: Urine chemistry of 3-month-old WT and KO mice. Averages of measurements from two consecutive 24 h urine collections. Cr = creatinine, d = 24 h, BW = body weight (g), Na^+, Cl^-, K^+, Ca^{2+}, Mg^{2+}, and Pi are normalised to individual creatinine levels of each mouse. Creatinine, total urinary protein, urea, uric acid, and glucose are normalised to 24 h urine production per bodyweight of each mouse. * $p < 0.05$, *** $p < 0.001$, mean ± SD, two-tailed T-test.

Parameter	Unit	WT	N	KO	N	*p*-value	
Na^+:Cr	mmol / mmol	37.32 ± 9.93	6	34.06 ± 12.57	6	0.6290	
Cl^-:Cr	mmol / mmol	70.18 ± 10.93	6	69.25 ± 19.70	6	0.9215	
K^+:Cr	mmol / mmol	50.25 ± 9.27	6	58.62 ± 8.86	6	0.1410	
Ca^{2+}:Cr	mmol / mmol	0.90 ± 0.55	6	6.48 ± 4.56	6	0.0140	*
Mg^{2+}:Cr	mmol / mmol	6.40 ± 1.81	4	8.05 ± 3.19	3	0.4184	
Pi:Cr	mmol / mmol	7.84 ± 2.98	6	22.45 ± 5.92	6	0.0003	***
Cr	µmol / (d * BW)	0.230 ± 0.038	6	0.221 ± 0.061	6	0.7548	
Total protein	µg / (d * BW)	197.43 ± 112.49	6	176.34 ± 104.42	6	0.7435	
Urea	µmol / (d * BW)	80.23 ± 21.42	6	80.42 ± 19.88	6	0.9876	
Uric acid	µmol / (d * BW)	37.33 ± 8.20	6	32.30 ± 11.60	6	0.4069	
Glucose	µmol / (d * BW)	0.133 ± 0.030	6	0.219 ± 0.178	6	0.2694	
24h urine	mg / h / BW	2.50 ± 0.56	6	2.98 ± 0.60	5	0.1999	

Table 3: Results of µCT analysis of hind-leg bones from 3-month-old WT and KO mice. Bone parameter abbreviations: Tb = trabecular bone at the distal femur, Ct = cortical bone at the tibio-fibular junction, TV = total volume, BV = bone volume, BV/TV = bone volume fraction, CD = connectivity density, SMI = structure model index, N = trabecular number, Th = thickness, Sp = spacing, BMD = bone mineral density. AU = arbitrary units. Mean ± SD, * $p < 0.05$, ** $p < 0.01$, two-tailed Student's t-test.

Parameter	Unit	WT	N	KO	N	*p*-value	
Tb.TV	mm³	2.13 ± 0.25	8	1.88 ± 0.15	9	0.0238	*
Tb.BV	mm³	0.33 ± 0,05	8	0.24 ± 0.04	9	0.0014	**
Tb.BV/TV	ratio	0.16 ± 0.02	8	0.13 ± 0.02	9	0.0133	*
Tb.CD	1/mm³	369.62 ± 39.79	8	285.25 ± 49.53	9	0.0016	**
Tb.SMI	AU	2.07 ± 0.28	8	2.37 ± 0.15	9	0.0123	*
Tb.N	1/mm³	5.91 ± 0.42	8	5.08 ± 0.80	9	0.0189	*
Tb.Th	µm	39.09 ± 5.94	8	37.30 ± 4.49	9	0.4915	
Tb.Sp	mm	0.17 ± 0.01	8	0.19 ± 0.02	9	0.0140	*
Tb.BMD	AU	1164.85 ± 8.75	8	1138.54 ± 23.69	9	0.0098	**
Ct.TV	mm³	0.40 ± 0.03	8	0.39 ± 0.04	9	0.3678	
Ct.BV	mm³	0.27 ± 0.02	8	0.25 ± 0.03	9	0.1977	
Ct.BV/TV	ratio	0.66 ± 0.03	8	0.66 ± 0.03	9	0.5431	
Ct.BMD	AU	1433.39 ± 33.25	8	1394.06 ± 16.96	9	0.0069	**
Ct.Th	µm	235.13 ± 15.15	8	226.56 ± 13.38	9	0.2344	

867 **Table 4: Comparison of the Klotho$^{-/-}$, PTG-CaSR$^{-/-}$, Renal-CaSR$^{-/-}$ and VSMC-CaSR$^{-/-}$**

868 **mice.** Arrows: (fold changes compared to control animals) =: no change, 1-2: ↓/↑; 2-3: ↓↓/↑↑;

869 >3: ↓↓↓/↑↑↑, n.d.: not determined

Parameter	**Klotho deficient** [54, 68]	**PTG-CaSR** $^{-/-}$ [18]	**Renal-CaSR**$^{-/-}$ [46]	**VSMC-CaSR**$^{-/-}$
Plasma Ca^{2+}	↑	↑↑	=	↑
Urinary Ca^{2+}	n.d.	↑↑↑	↓↓↓	↑↑↑
Plasma Pi	↑	n.d.	=	↓
Urinary Pi	↑	n.d.	n.d.	↑↑
Plasma 1,25-D_3	↑↑	n.d.	=	↑↑
Plasma PTH	↓	↑↑↑	=	↑
FGF23	↑↑	n.d.	n.d.	↑↑
Body weight	↓↓	↓↓↓	=	=/↓
BMD	↓	↓↓↓	=	↓

870

Figure legends

Figure 1: *In vitro* calcification of isolated VSMC. A: Photograph of 24-well microplates with cultured VSMC from WT (left two plates) and KO mouse aortas (right two plates) incubated for 10 days with a series of Ca^{2+} (numbers: mM Ca^{2+} in the 3 horizontally adjacent wells) / phosphate (Pi) concentrations (top two plates: 2 mM Pi, bottom two plates: 3 mM Pi) in the growth medium. Cells were then fixed and stained with Alizarin Red S. Darker spots indicate calcium deposits. At 2 mM Pi, WT did not show any calcification independent of the Ca^{2+} concentration, while VSMC from KO mice started to show calcification at 1.6 mM Ca^{2+}. At 3 mM Pi, WT cells started to calcify at 1.6 mM Ca^{2+} and KO cells at 1.2 mM Ca^{2+}. **B:** Quantification of Ca^{2+} deposition in WT and KO cells at 3 mM Pi and 1.2, 1.8 or 2.5 mM Ca^{2+} using o-cresolphthalein complexone assay, normalised to the amount of protein (BCA assay) and the normocalcemic (1.2 mM Ca^{2+}) control. Friedmann with Dunn post-hoc test. **C:** Quantification of Ca^{2+} deposition in WT and KO cells at 3 mM Pi and 1.2 mM Ca^{2+} in the presence or absence of 10 nM calcimimetic R-568. Median±IQR, Mann-Whitney-U test. * $p < 0.05$, ** $p < 0.01$.

Figure 2: Aorta mRNA expression levels and quantitative immunohistochemistry. A: *Klotho*, **B:** *Cyp27b1*, and **C:** *Sm22α* mRNA expression levels relative to calibrator (mean ΔCT WT). **D & E:** quantitative immunohistochemistry analysis of α-Klotho in smooth muscle and endothelial layer of WT and KO aorta sections. Mean grey values (lower = darker). **F:** representative stainings for α-Klotho used for quantification. **G & H:** quantitative immunohistochemistry analysis of CYP27B1 in smooth muscle and endothelial layer of WT and KO aorta sections. Mean grey values (lower = darker). **I:** representative stainings for CYP27B1 used for quantification. Inserts = IgG negative control. Inserts = IgG negative control. Scale bars = 50 µm.

Figure 3: Kidney calcium handling and CaSR expression in $^{SM22\alpha}CaSR^{\Delta flox/\Delta flox}$ mice. A-B: semi-quantitative Western blot analyses of □-Klotho and the sodium phosphate cotransporter, NaPi2a. **C-F:** quantitative immunohistochemistry of the vitamin D receptor (VDR), the calcium channel Transient Receptor Potential cation channel subfamily V member 5 (TRPV5), calbindin (D28K) and the plasma membrane calcium ATPase (PMCA). **G:** CaSR mRNA expression in whole kidney lysate relative to calibrator (mean ΔCT of WT). **H:** quantitative immunofluorescence analysis of CaSR expression in kidney sections. **I:** semi-quantitative Western blot analysis of CaSR protein expression in whole kidney lysates. Mean±SD, * $p < 0.05$, ** $p < 0.01$, *** $p < 0.001$, two-tailed Student's t-test.

Figure 4: Kidney water transport in $^{SM22\alpha}CaSR^{\Delta flox/\Delta flox}$ mice. A: Optical microscopy images of crystal precipitates in urines from WT and KO mice (scale bar: 100 µm). **B:** Urine osmolality and **C:** urine pH of WT and KO mice from two consecutive days in metabolic cages. Mean±SD, ** $p < 0.01$, *** $p < 0.001$ for overall genotype effect, two-way ANOVA. **D-H:** semi-quantitative Western blot analyses of the thiazide sensitive sodium-chloride cotransporter (NCC), V-H^+-ATPase, total aquaporin 2 (AQP2), pS261-AQP2, pS256-AQP2 in WT and KO kidney lysates. **I:** AQP2 excretion measured by ELISA assay in urines from WT and KO. Mean±SD, * $p < 0.05$, ** $p < 0.01$, two-tailed Student's t-test.

Figure 5: **Analysis of the parathyroid glands. A**: Micrographs of isolated parathyroid glands from WT and KO mice. Scale bar = 500 µm. **B**: Immunofluorescence images of isolated parathyroid glands from WT and KO mice, showing comparable staining intensity for the CaSR. Scale bar = 50 µm. **C**: Western Blot analysis of CaSR expression in parathyroid glands, showing equal expression of both the monomer (~130 kDa) and the dimer (~250 kDa) of the CaSR. **D**: PTH release assay in response to increases in extracellular Ca^{2+}. Left panel: raw data,

right panel: normalised to PTH release at 0.5 mM Ca^{2+} = 100 % for both WT and KO. Vertical lines indicate Ca^{2+} concentration at half maximal PTH response. N = 3, < 1.4 % total variance explained by genotype as determined by repeated measures two-way ANOVA.

Figure 6: Phenotype of the $^{SM22\alpha}$CaSR$^{\Delta flox/\Delta flox}$ mice. Continuous lines = stimulation, broken lines = inhibition. Greyed out lines = loss of action due to VSMC-CaSR deletion.
Loss of the CaSR in VSMC affects whole body mineral ion homeostasis leading to the loss (red X signs) of an inhibitory function on the production / secretion of 1,25-D_3, PTH, and FGF23. At the same time, VSMC-CaSR loss apparently also affects or overrides hormonal control: 1,25-D3 synthesis is apparently resistant to control by FGF23, while PTH secretion is (slightly) increased, pointing to some degree of resistance to control by 1,25-D_3, FGF23, and serum calcium (despite a fully functional CaSR in the parathyroid glands). The increased 1,25-D_3 and PTH leads to hypercalcemia followed by hypercalciuria. Pi excretion is increased as a result of the increased PTH and FGF23 levels, leading to low serum Pi. Urine osmolality and pH are decreased to prevent nephrolithiasis. The urinary calcium and phosphate wasting then contributes to the observed bone loss in these animals (not shown in the scheme). Owing to the presence of blood vessels in all organs of the body, it remains to be elucidated whether all the observed features of this phenotype are primary to CaSR deletion from the VSMC, secondary compensatory mechanisms, or a combination of both.

Figure 1

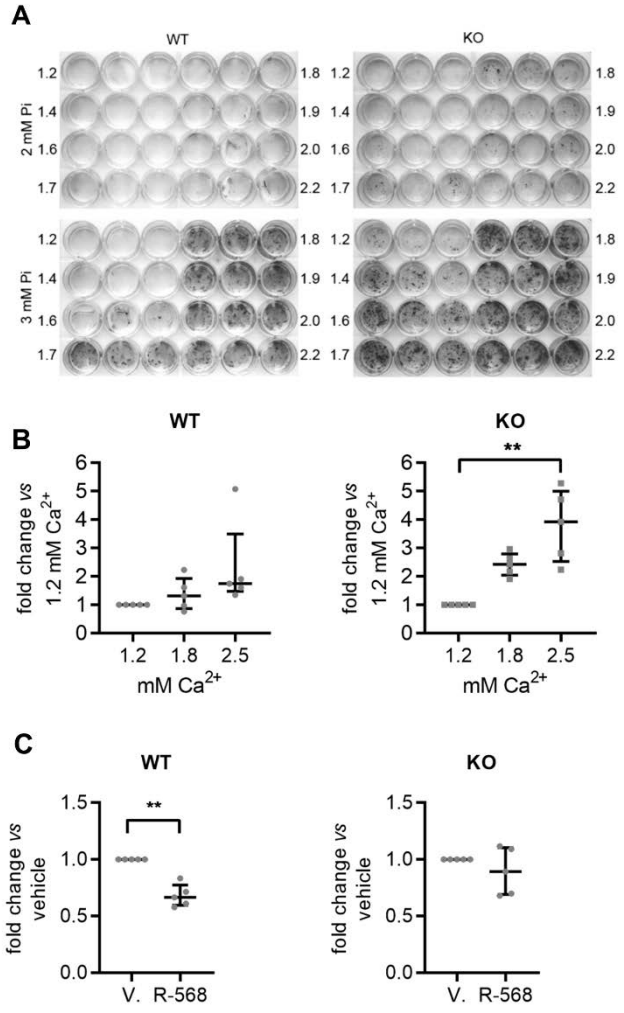
A
WT
KO
2 mM Pi
3 mM Pi
1.2
1.4
1.6
1.7
1.8
1.9
2.0
2.2
B
WT
KO
**
fold change vs 1.2 mM Ca2+
mM Ca2+
1.2
1.8
2.5
C
WT
KO
**
fold change vs vehicle
V.
R-568

Figure 2

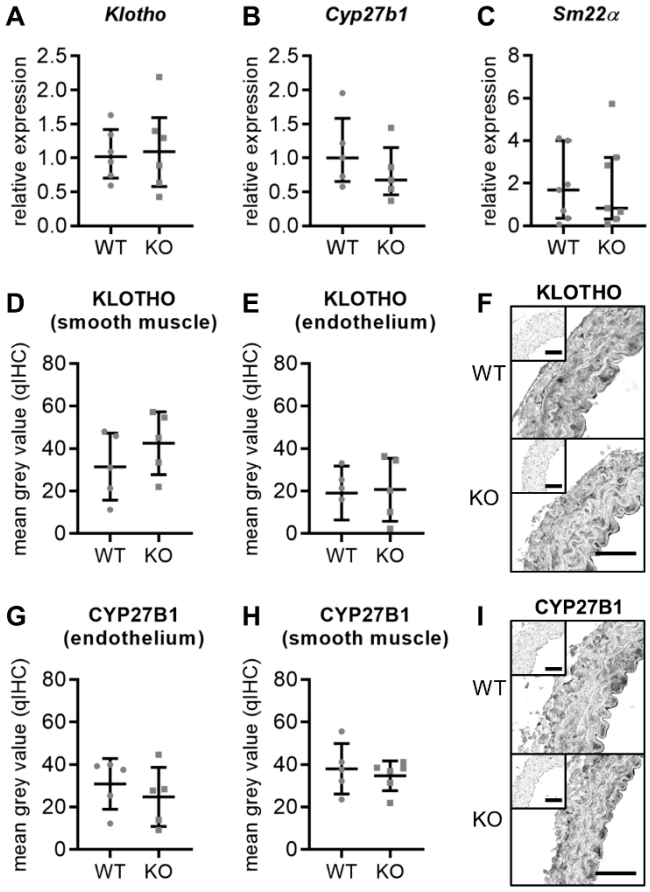
A
Klotho
relative expression
2.5
2.0
1.5
1.0
0.5
0.0
WT
KO
B
Cyp27b1
relative expression
2.5
2.0
1.5
1.0
0.5
0.0
WT
KO
C
Sm22α
relative expression
8
6
4
2
0
WT
KO
D
KLOTHO
(smooth muscle)
mean grey value (qIHC)
80
60
40
20
0
WT
KO
E
KLOTHO
(endothelium)
mean grey value (qIHC)
80
60
40
20
0
WT
KO
F
KLOTHO
WT
KO
G
CYP27B1
(endothelium)
mean grey value (qIHC)
80
60
40
20
0
WT
KO
H
CYP27B1
(smooth muscle)
mean grey value (qIHC)
80
60
40
20
0
WT
KO
I
CYP27B1
WT
KO

Figure 3

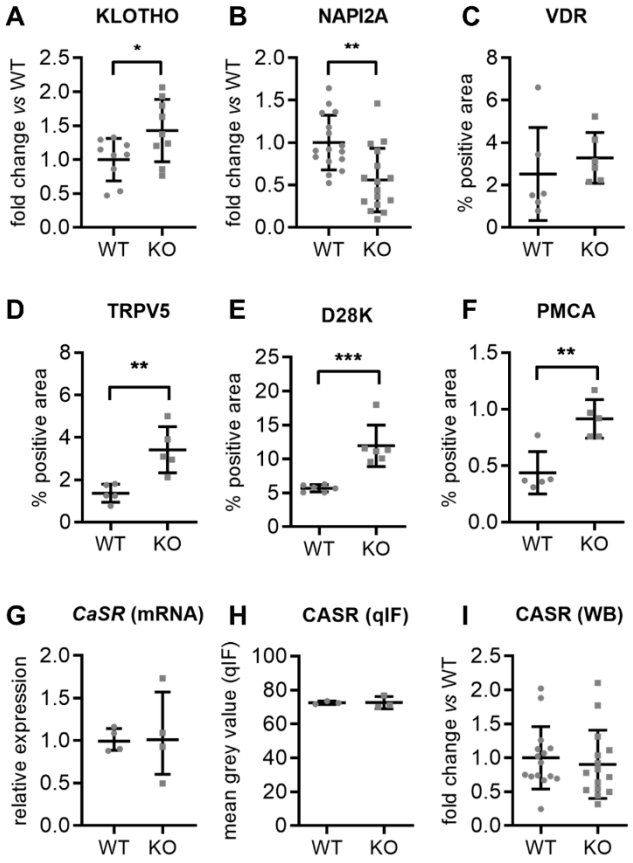
A
KLOTHO
fold change vs WT
*
WT
KO
B
NAPI2A
fold change vs WT
**
WT
KO
C
VDR
% positive area
WT
KO
D
TRPV5
% positive area
**
WT
KO
E
D28K
% positive area
***
WT
KO
F
PMCA
% positive area
**
WT
KO
G
CaSR (mRNA)
relative expression
WT
KO
H
CASR (qIF)
mean grey value (qIF)
WT
KO
I
CASR (WB)
fold change vs WT
WT
KO

Figure 4

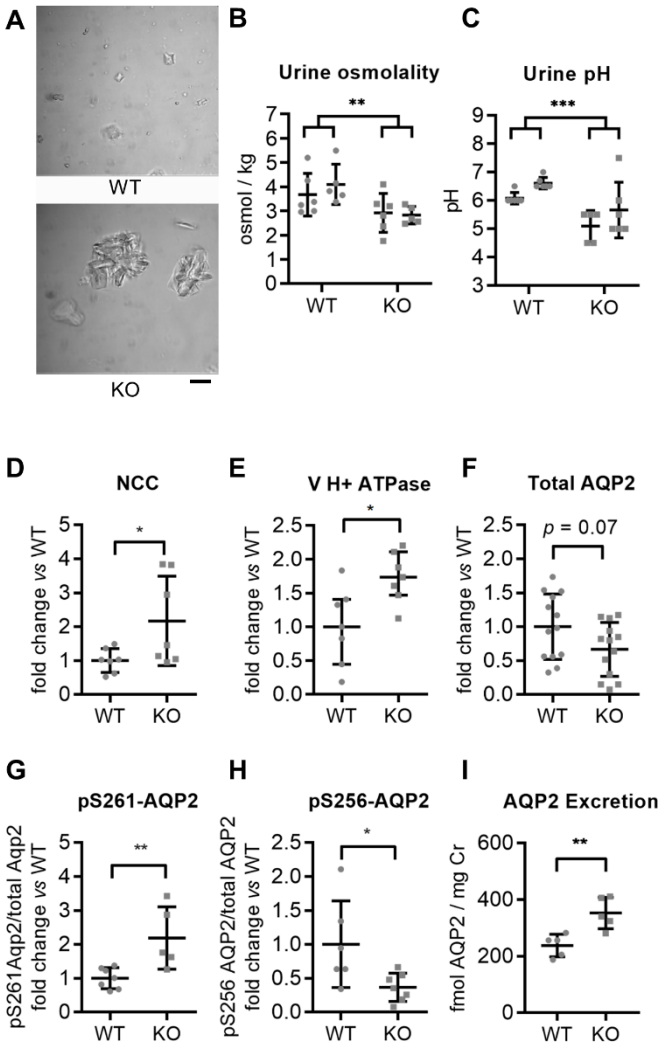
A
WT
KO
B
Urine osmolality
osmol / kg
**
WT
KO
C
Urine pH
pH
***
WT
KO
D
NCC
fold change vs WT
*
WT
KO
E
V H+ ATPase
fold change vs WT
*
WT
KO
F
Total AQP2
fold change vs WT
p = 0.07
WT
KO
G
pS261-AQP2
pS261Aqp2/total Aqp2 fold change vs WT
**
WT
KO
H
pS256-AQP2
pS256 AQP2/total AQP2 fold change vs WT
*
WT
KO
I
AQP2 Excretion
fmol AQP2 / mg Cr
**
WT
KO

Figure 5

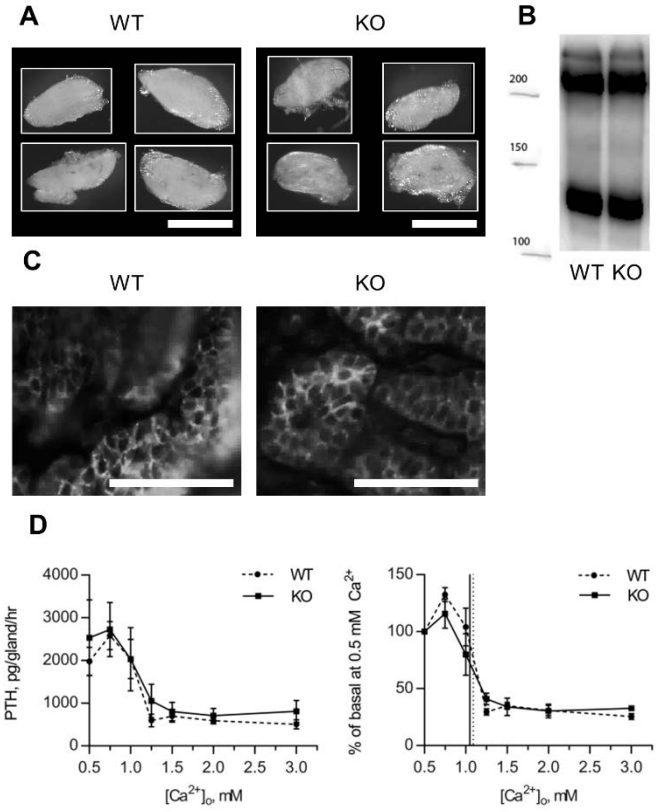
A
WT
KO
B
200
150
100
WT KO
C
WT
KO
D
PTH, pg/gland/hr
4000
3000
2000
1000
0
WT
KO
0.5 1.0 1.5 2.0 2.5 3.0
[Ca2+]o, mM
% of basal at 0.5 mM Ca2+
150
100
50
0
WT
KO
0.5 1.0 1.5 2.0 2.5 3.0
[Ca2+]o, mM

Figure 6

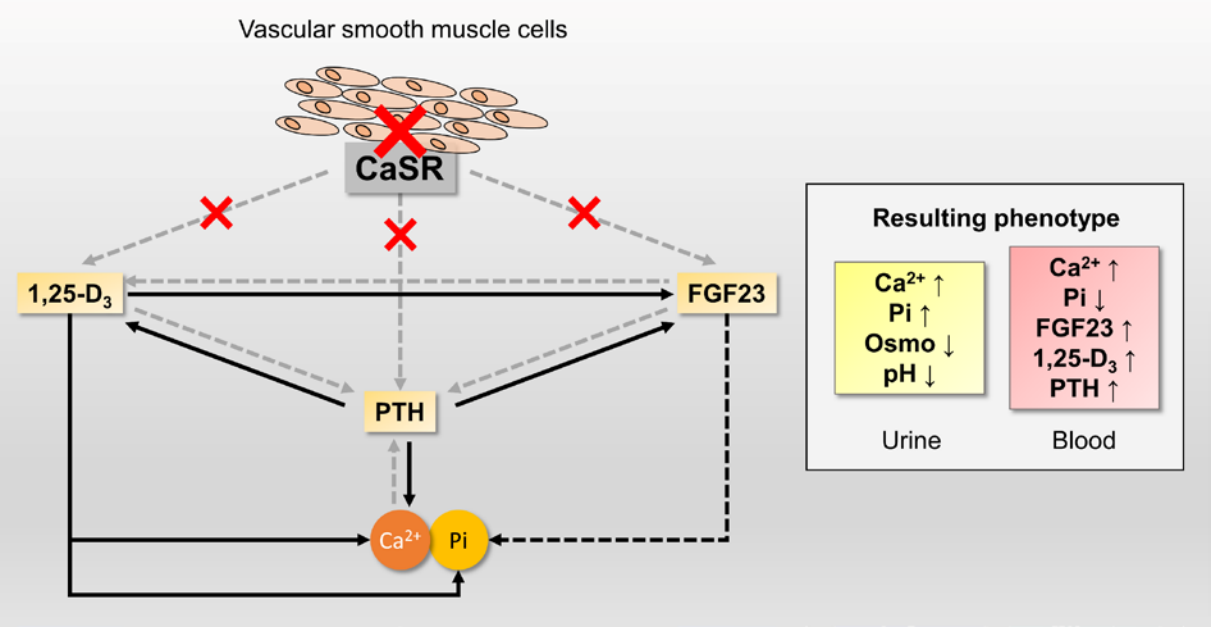
Vascular smooth muscle cells
CaSR
1,25-D3
FGF23
PTH
Ca2+
Pi
Resulting phenotype
Ca2+ ↑
Pi ↑
Osmo ↓
pH ↓
Urine
Ca2+ ↑
Pi ↓
FGF23 ↑
1,25-D3 ↑
PTH ↑
Blood

Supplemental material

Table of contents

Table S1: Blood biochemistry of 18-month-old WT and KO mouse. * $p < 0.05$, ** $p < 0.01$, mean ± SD, two-tailed T-test. "CaSR" indicates concentration of N-terminal soluble CaSR / CaSR-fragment. Osmolality and CaSR were measured in male and female mice.

Parameter	Unit	WT	N	KO	N	*p*-value	
Na^+	mmol / l	149.0 ± 3.61	3	146.3 ± 3.06	3	0.3837	
K^+	mmol/l	10.64 ± 0.61	3	11.88 ± 2.53	3	0.4541	
Cl^-	mmol / l	114.33 ± 1.15	3	111.00 ± 3.61	3	0.2020	
Ca^{2+}	mmol / l	2.34 ± 0.13	3	2.99 ± 0.35	3	0.0401	*
Mg^{2+}	mmol / l	1.65 ± 0.18	3	2.04 ± 0.33	3	0.1369	
FGF23	pg / ml	131.1 ± 45.5	3	330.0 ± 49.7	3	0.0069	**
α-Klotho	pg / ml	2005.9 ± 1342.1	4	1873.0 ± 1016.5	4	0.8797	
Osmolality	mosmol/kg	289.2 ± 11.7	5	288.1 ± 5.6	7	0.8369	
CaSR	ng / ml	2.17 ± 0.98	5	2.03 ± 0.78	7	0.7816	

Table S2: Organ weights of 6 and 18-month-old animals. WT *vs*. KO, mean ± SD, two-tailed T-test.

Organ	**Unit**	**WT**	**N**	**KO**	**N**	***p*-value**
6-month-old animals						
Kidney	mg	235.0 ± 32.3	7	232.9 ± 23.8	7	0.8899
Liver	mg	1332.2 ± 134.2	8	1445.6 ± 190.9	7	0.2016
Stomach	mg	339.4 ± 86.8	8	444.6 ± 256.8	7	0.2938
Spleen	mg	88.1 ± 31.3	8	99.1 ± 34.3	6	0.5467
Heart	mg	148.8 ± 31.0	8	145.4 ± 17.7	6	0.8144
18-month-old animals						
Kidney	mg	313.1 ± 37.6	6	313.0 ± 12.9	4	0.9950
Liver	mg	2294.1 ± 461.2	6	2399.8 ± 107.9	4	0.6703
Stomach	mg	846.8 ± 372.0	6	738.8 ± 247.6	4	0.6268
Spleen	mg	129.1 ± 52.6	6	101.6 ± 24.8	4	0.3637
Heart	mg	201.8 ± 20.4	5	231.9 ± 8.4	4	0.0285 *

Figure S1: Generation of explant derived aortic VSMC. A: The thoracic aorta is dissected from the spine and **B:** removed to a Petri dish filled with sterile isolation medium where **C and D:** the vessel is cleared from tunica adventitia by gently pulling / scraping the connective tissue until **E:** only the semi-translucent tunica media remains. **F:** The vessel is then cut into small (ca. 1 mm) pieces that are then **G:** transferred into a T-25 cell culture flask by the use of a hypodermic needle. **H:** The flask is kept in an upright position at 37 °C for 10–15 minutes so that the explants are not in contact with medium and can attach firmly to the surface of the flask. 5 ml isolation medium is added, and the explants are kept at 37 °C / 95 % relative humidity (rh) / 5 % CO2 for ca. 7 days after which the medium is changed. **I:** VSMC will start to grow out of the explants. **J:** After ca. 2-3 weeks, the explants are removed and the VSMC passaged to generate a monolayer of cells.

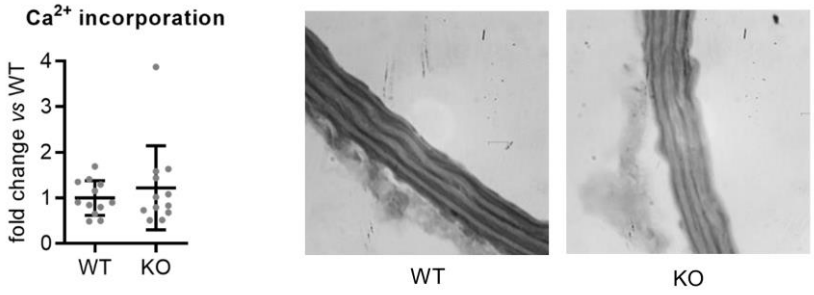

Figure S2: ***Ex vivo*** **aortic calcification.** Graph: Quantification of Ca^{2+} deposition in WT and KO aortas or 3-month-old mice. Mean±SD. Pictures: Alizarin Red S stainings of thoracic aorta sections from 12-month-old WT and KO animals incubated for 10 days in the presence of medium containing 1.8 mM Ca^{2+} and 3 mM Pi.

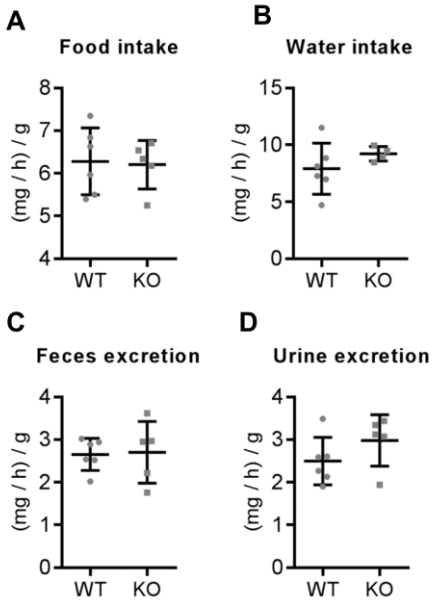

Figure S3: Metabolic cage studies of WT and KO mice. A. Food intake, **B**: Water intake, **C**: Feces excretion, **D**: Urine excretion. Data are shown as consumption (in mg) per h per g bodyweight. Mean±SD.

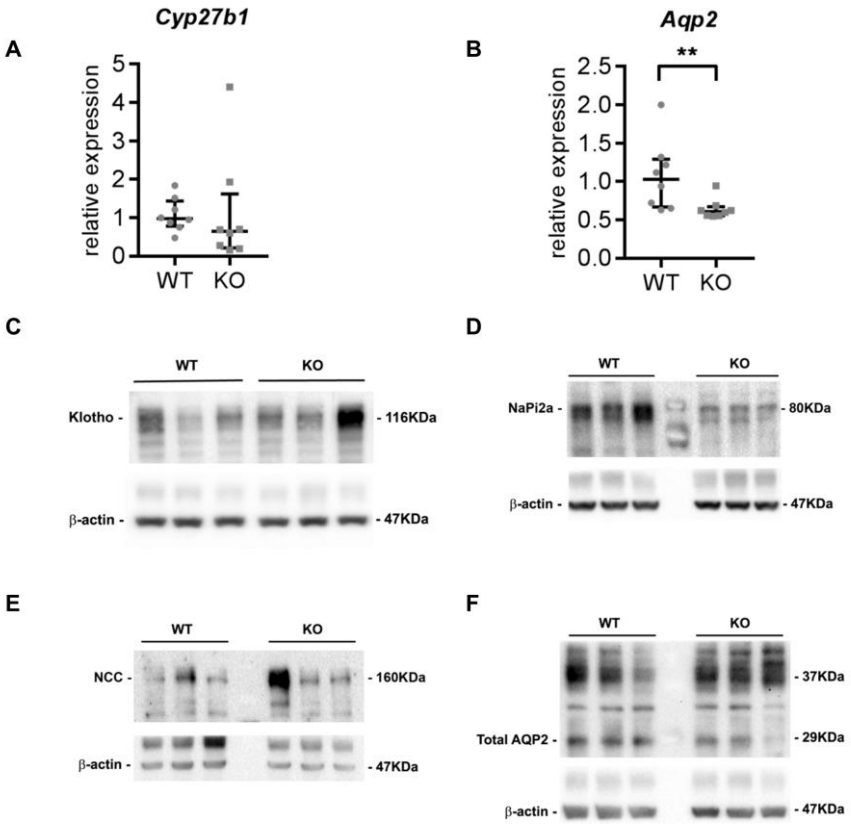

Figure S4: **Supplemental kidney mRNA and protein expression. A:** *Cyp27b1*, and **B:** *Aqp2* mRNA expression levels relative to calibrator (mean ΔCT WT). Representative Western blots showing **C:** Klotho, **D:** NaPi2a, **E:** NCC, **F:** AQP2 expression in kidneys from WT and KO mice.

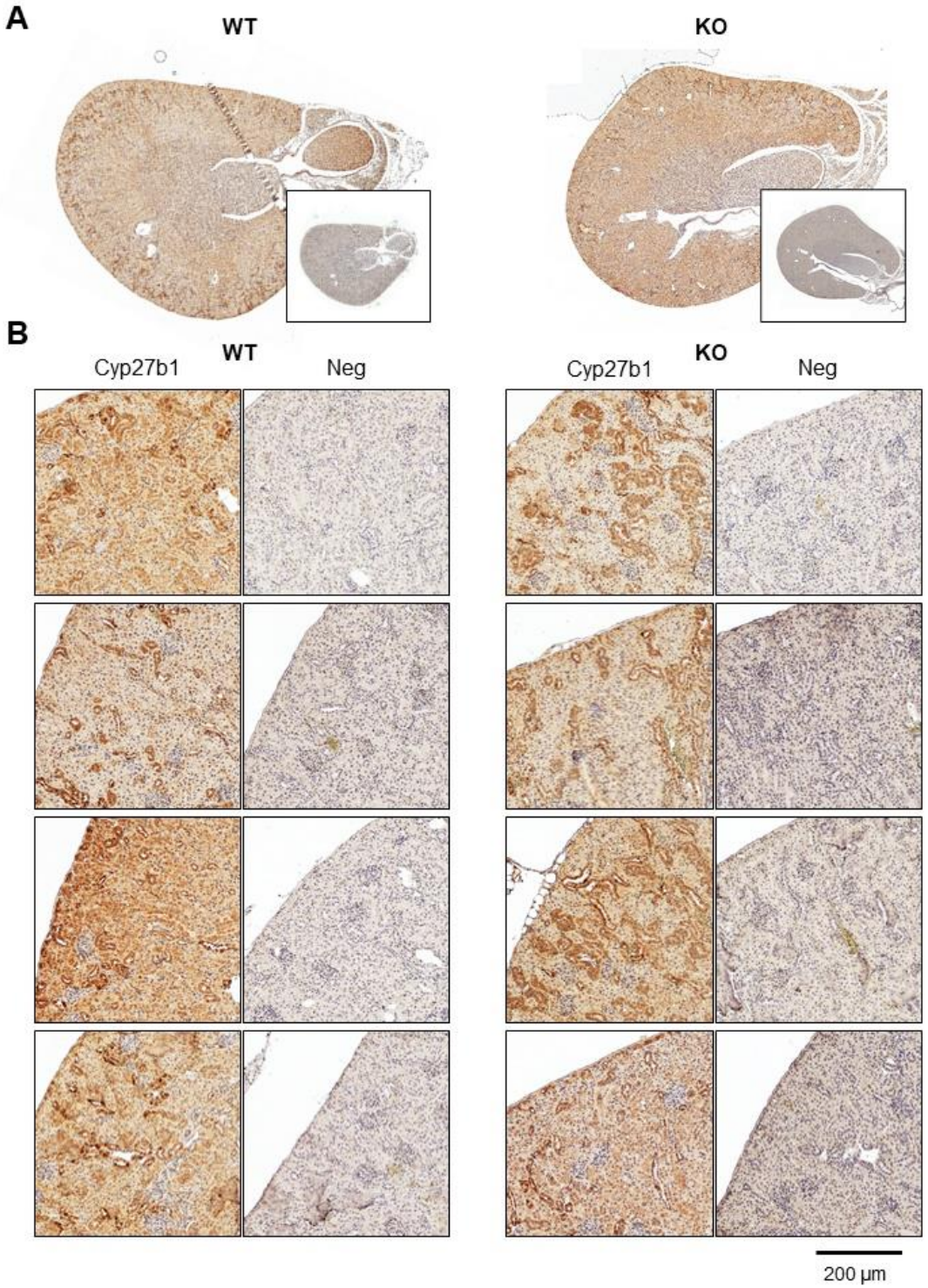

Figure S5: Immunohistochemistry stainings of Cyp27b1 in kidneys of WT and KO mice. Stainings were performed as described in the methods section for Cyp27b1 using the LSBio (Seattle, USA) rabbit anti-Cyp27b1 antibody at 1:1000 dilution. **A:** Overview of representative whole kidney sections stained for Cyp27b1. Insert: negative control. **B:** Cortex of N=4 WT and KO kidneys stained for Cyp27b1 and respective negative controls.

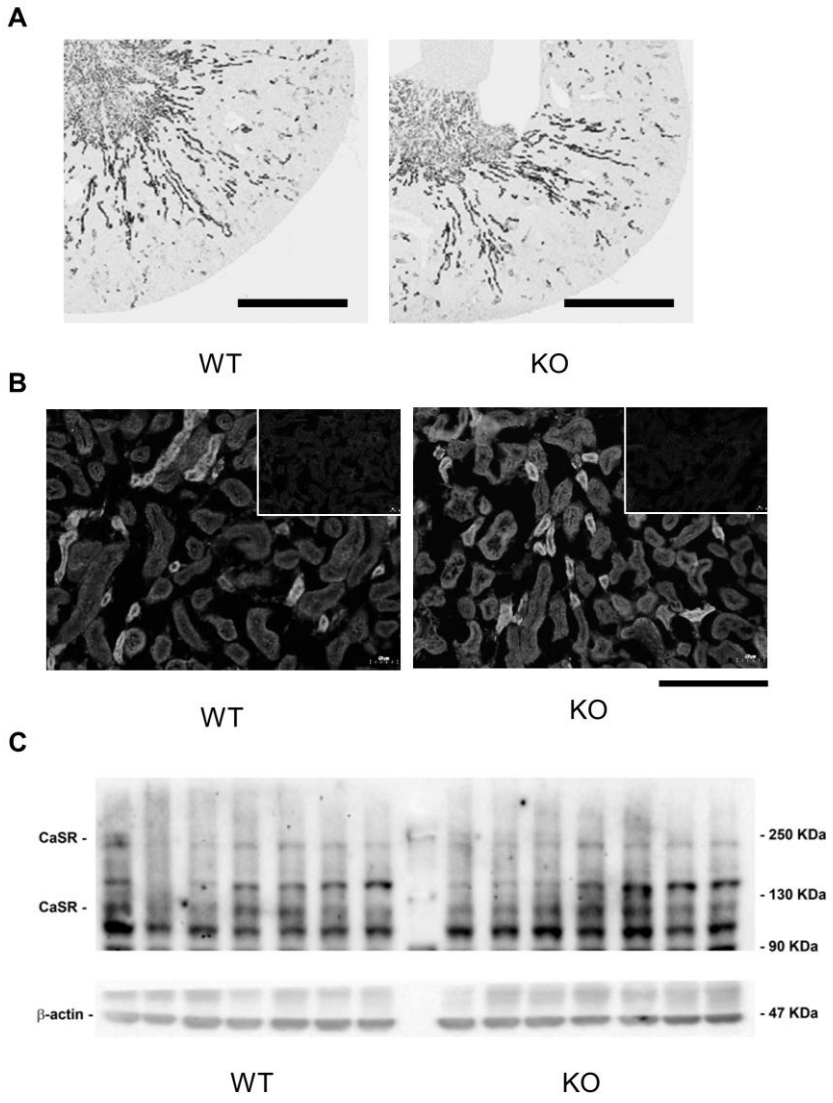

Figure S6: Supplemental kidney CaSR expression data and representative images from Figure 3. A: immunohistochemistry of CaSR expression pattern in WT and KO kidney sections. Scale bar = 1 mm. **B:** immunofluorescence analysis of CaSR expression levels in WT and KO kidneys used for quantitative immunofluorescence analysis. Scale bar = 200 µm. **C:** representative Western blot for CaSR in the kidney (~120-150 kDa: monomer; 250 kDa: dimer).

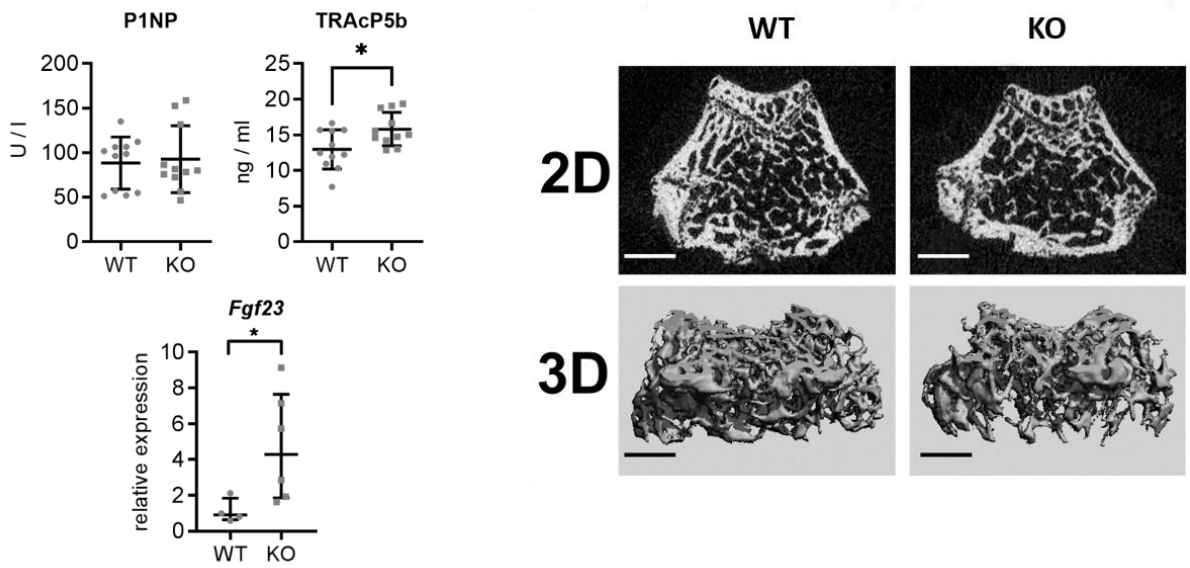

Figure S7: Plasma levels of bone metabolism markers procollagen type 1 (P1NP) and Tartrate-resistant acid phosphatase 5b (TRAcP5b), Fgf23 mRNA expression in bone, and µCT. Bone metabolism markers: * $p < 0.05$, two tailed T-test; measured in male and female mice. RT-qPCR: * $p < 0.05$, Mann-Whitney test. µCT: representative 2-dimension (2D) radiographs and 3-dimension (3D) reconstructed images from distal femurs of 3 months old KO and WT (control) littermates. The 2D radiographs were taken 100 µm below the growth plate. Scale bar: 400 µm

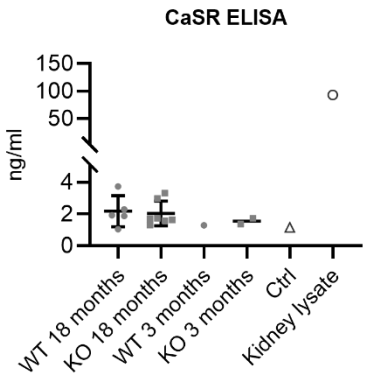

Figure S8: Serum levels of "soluble" CaSR / CaSR fragment. N = 5 (WT, 18 months), N = 7 (KO, 18 months), N = 3 (WT, 3 months), and N = 3 (KO, 3 months). Three of the 3-month samples, (2 WT, 1 KO) were below the detection range and are thus not included in the graph. An additional serum sample of a genetically non-modified 14 month-old mouse ("Ctrl") was added for reference, which had a comparable level of CaSR in the serum. Finally, a sample of 100 mg / ml kidney lysate from a genetically non-modified mouse was tested as positive control.